SYNTHESIS AND REACTIVITY OF THE BIS(PHENYLIMINIO)PYRIDINE IRON BIS(DINITROGEN) COMPLEX: CATALYST DEACTIVATION VIA ARENE COORDINATION

A Thesis

Presented to the Faculty of the Graduate School

of Cornell University

In Partial Fulfillment of the Requirements for the Degree of

Master of Science

by

Andrew Milbank Archer

August 2006

ABSTRACT

In pursuit of highly active iron-based catalysts for bond-forming reactions, the phenyl-substituted bis(phenylimino)pyridine iron bis(dinitrogen) complex, (^{iPr}PhPDI)Fe(N_2)$_2$ (^{iPr}PhPDI = 2,6-(2,6-($CHMe_2$)$_2C_6H_3N$=CC_6H_5)$_2C_5H_3N$), was prepared by sodium amalgam reduction of the ferrous dichloride precursor under four atmospheres of dinitrogen. The bis(dinitrogen) compound displayed catalytic productivity for the hydrogenation and hydrosilation of 1-hexene superior to that of the methyl-substituted analog, (^{iPr}PDI)Fe(N_2)$_2$ (^{iPr}PDI = 2,6-(2,6-($CHMe_2$)$_2C_6H_3N$=CCH_3)$_2C_5H_3N$). However, the catalytic productivity with more hindered substrates, such as cyclohexene and (R)-(+)-limonene, was inferior. The diminished catalytic productivity with these substrates precipitated from competitive deactivation via irreversible formation of η^6-aryl and -phenyl complexes unobserved in the chemistry of (^{iPr}PDI)Fe(N_2)$_2$. Dissolution of (^{iPr}PhPDI)Fe(N_2)$_2$ in coordinating solvents such as THF or cyclohexene prompted exclusive formation of the η^6-phenyl derivative, whereas dissolution in non-coordinating solvents such as pentane, ether, and mesitylene afforded solely the η^6-aryl compound.

A family of bis(imino)pyridine ligands bearing alkylimino-substituents (rather than arylimino-substituents) was also synthesized and complexed to ferrous dibromide. Conversion to the corresponding dicarbonyl compounds was affected by sodium amalgam reduction under four atmospheres of carbon monoxide. Electronic studies of these alkylimino-substituted bis(imino)pyridine iron dicarbonyls demonstrated the electron-donating character of the ligands relative to their arylimino-substituted counterparts. Initial attempts to isolate effective precatalysts for C-H bond-forming reactions bearing the alkylimino-substituted bis(imino)pyridine ligand were unsuccessful. However, through the course of these attempts, a new precatalyst

bearing the arylimino-substituted ^{Et}PDI ligand (^{Et}PDI = (2,6-(2,6-$Et_2C_6H_3N{=}CMe)_2C_5H_3N$) was isolated by sodium amalgam reduction in the presence of excess 1,3-butadiene. The catalytic productivity of this butadiene complex for hydrogenation of simple olefins was assayed. An induction period was identified, and its origins examined.

BIOGRAPHICAL SKETCH

Andrew Archer graduated from Groton School in 2000 and attended Duke University in Durham, North Carolina. There he tasted the excitement and frustration of chemical research in the laboratories of Professors Jie Liu and Stephen Craig. Although he had little success in lab work, his distinguished marks and enthusiasm put him in good standing with the faculty, who presented him with the Department of Chemistry Award upon his graduation Magna Cum Laude and Phi Beta Kappa in 2004.

Afloat in propaganda surrounding the nascent 'nanotechnology industry,' Andrew arrived at Cornell hoping to catch the swelling nanotech wave and ride it to fortune. However, his coursework exposed him to a dissimilar, more interesting fields. After some deliberation, he decided to try his hand at research in synthetic organometallic chemistry, and joined the lab of Professor Paul Chirik.

During his two-year stint as a student, teacher, and researcher at Cornell, Andrew gained a competency in the field of organometallic chemistry but also learned a great deal about himself. He discovered that his passions lay not in laboratory research and the implicit synthesis of data, but in creative uses and salable applications of information. Consequently, Andrew decided, after what was arguably a successful research tenure, to graduate from Cornell with a Masters Degree and sample vocations outside of research.

To my mother, my family, and friends,

many of whom will understand not a word of this document.

ACKNOWLEDGMENTS

I would first like to thank my advisor, Professor Paul Chirik, who piloted me through my research. I assume that his wits were often tested by the data that I presented him with. So, I must partially credit the assiduousness of this report to his profound knowledgebase, his passion for chemical experimentation, and his frequent exacerbation.

I'd like to acknowledge Professors Peter Wolczanski and Bruce Ganem, who served on my special committee. I credit both for inspiration in and outside of chemical research.

Professionally, I would also like to thank the NMR support staff, Anthony Condo and Ivan Keresztes, as well as our distinctive crystallographer Emil Lobkovsky. I will forget neither the excitement of bringing Emil crystals for analysis, nor the confusing, somewhat theatrical suspense he created while I waited to learn if the crystals I brought him would diffract.

For their help in the laboratory, their humor and commiseration, I would like to thank my coworkers in the Chirik Group, particularly Suzanne Bart, Wesley Bernskoetter, Chris Bradley, Tamara Hanna, and Ryan Trovitch. I sincerely wish them all well in their research careers. I know they all have the ethics and passions to succeed.

I could not have made do as a graduate student for two years in frigid Ithaca, New York without the wild cast of classmates and friends I was fortunate to know. Among them: Sungsoo Yoo, Ryan Trovitch, Mahendra Orilall, Ethan Chiang, Amanda Bowman, and Mike Airola. If graduate school was truly the hangover from college, they were the aspirin.

Finally, and importantly, I would like to thank my mother, Elizabeth, my sister, Hilary, my remaining family, and Meghan Miller, my girlfriend and resolved supporter through most of graduate school. Suffice it to say that I would not be the person I am or where I am today without them.

TABLE OF CONTENTS

LIST OF FIGURES

LIST OF TABLES

Chapter 1

Synthesis and Reactivity of the Bis(phenylimino)pyridine Iron Bis(dinitrogen) Complex: Catalyst Deactivation Via Arene Coordination

1.1 Abstract

The phenyl-substituted bis(phenylimino)pyridine iron bis(dinitrogen) complex, (^{iPr}PhPDI)Fe(N_2)$_2$ (^{iPr}PhPDI = 2,6-(2,6-($CHMe_2$)$_2C_6H_3N$=CC_6H_5)$_2C_5H_3N$), was prepared by sodium amalgam reduction of the ferrous dichloride precursor under four atmospheres of dinitrogen. The bis(dinitrogen) compound displayed catalytic productivity for the hydrogenation and hydrosilation of 1-hexene superior to that of the methyl-substituted analog, (^{iPr}PDI)Fe(N_2)$_2$ (^{iPr}PDI = 2,6-(2,6-($CHMe_2$)$_2C_6H_3N$=CCH_3)$_2C_5H_3N$). However, the catalytic productivity with more hindered substrates, such as cyclohexene and (R)-(+)-limonene, was inferior. The diminished catalytic productivity with these substrates was a consequence of competitive deactivation resulting from irreversible formation of η^6-aryl and -phenyl complexes unobserved in the chemistry of (^{iPr}PDI)Fe(N_2)$_2$. Dissolution of (^{iPr}PhPDI)Fe(N_2)$_2$ in coordinating solvents such as THF or cyclohexene prompted exclusive formation of the η^6-phenyl derivative, whereas dissolution in non-coordinating solvents such as pentane, ether, and mesitylene afforded solely the η^6-aryl compound.

1.2 Introduction

Catalytic bond forming reactions mediated by well-defined, homogeneous, transition-metal complexes find increasing use in synthetic chemistry.[1,2,3] Highly selective catalytic transformations are now efficiently conducted on substances bearing even the most reactive functionalities.[4,5,6] Commonly, the most useful

catalysts contain late second- and third-row transition metals which are significantly more toxic and expensive than their first-row counterparts.[7] A salient pursuit in organometallic chemistry is, therefore, the development of catalysts with comparable activity and selectivity that are based on first-row transition metals. Particularly attractive is iron, given its high terrestrial abundance, reasonable price, and low toxicity.[8]

Iron species have been known to catalyze a variety of organic transformations, including C-C cross-coupling reactions[9,10] and olefin polymerizations[11] and hydrogenations.[12] However, the identities of the catalytically active species have been poorly understood. In one exception, Wrighton and coworkers reported evidence, later corroborated by Weitz,[13] suggesting the fourteen electron intermediate [$Fe(CO)_3$] was the active species in photocatalytic hydrogenation, hydrosilation and isomerization of olefins with [$Fe(CO)_5$].[14,15] Our group theorized that the terdentate scaffold of a new class of bis(imino)pyridine ligands, found to support highly active iron and cobalt catalysts for olefin polymerization,[16,17] could provide the correct geometry and spin-state to mimic the active tri-(carbonyl) fragment under mild thermal conditions.

Reduction of the diisopropyl-aryl bis(methylimino)pyridine iron dibromide, ^{iPr}PDIFeBr$_2$ (^{iPr}PDI = 2,6-(2,6-$(CHMe_2)_2C_6H_3N{=}CCH_3)_2C_5H_3N$) (**1-Br$_2$**), yielded the corresponding bis(dinitrogen) compound, ^{iPr}PDIFe$(N_2)_2$ (**1-$(N_2)_2$**), which proved to be a thermally stable, highly active pre-catalyst for hydrogenation and hydrosilation of olefins.[18] The stability and catalytic activity of the complex has been attributed to the ligand's capacity to accept up to three electrons[19] from the metal center through conjugated π-acidic nitrogen atoms to mitigate the one electron redox changes intrinsic to iron.[20] Indeed, examination of the electronic structure of **1-$(N_2)_2$** with Mössbauer spectroscopy, SQUID magnetometry, DFT calculations, and a survey of metrical parameters established the redox non-innocence of the bis(imino)pyridine

ligand in the complex (Figure 1.1), which is formulated as an intermediate spin ferrous center with a doubly reduced bis(imino)pyridine dianion.[21]

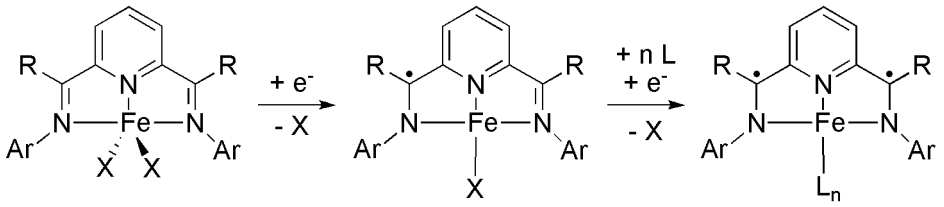

Figure 1.1: Redox non-innocence of the bis(imino)pyridine ligand (R = Me, Ph).

This chapter describes the synthesis and study of the phenyl-substituted bis(imino)pyridine iron bis(dinitrogen) complex, (^{iPr}PhPDI)Fe(N_2)$_2$ (^{iPr}PhPDI = 2,6-(2,6-(CHMe$_2$)$_2$C$_6$H$_3$N=CC$_6$H$_5$)$_2$C$_5$H$_3$N) (**2-(N_2)$_2$**). Owing to the extended π-conjugation in the backbone and increased capacity for metal-ligand electron transfer,[22] we anticipated that **2-(N_2)$_2$** would exhibit catalytic activity which improved upon that of **1-(N_2)$_2$**. The replacement of the backbone methyl-substituents with phenyl-substituents was also expected to provide greater stability to the complex and guard against undesirable deprotonation of the methyl-backbone.[23,24,25] Moreover, the phenyl-substituted complex was an ideal target, given the relative ease with which its dichloride precursor could be synthesized.[26] Changes in structure, electronic properties and catalyst performance were evaluated, and through the course of these studies, an important catalyst deactivation pathway was elucidated.

1.3 Results and Discussion

Synthesis and Characterization of (^{iPr}PhPDI)FeX$_2$

Synthesis of bis(imino) pyridine ligand with phenyl backbone substituents was accomplished in moderate yield (54%) by condensation of 2,6-dibenzoylpyridine (prepared by Friedel-Crafts acylation of benzene[27] with the pyridine-2,6-dicarbonyl

dichloride[28]) with 2,6-diisopropyl aniline under forcing conditions.[26] The ligand was metallated to afford (^{iPr}PhPDI)FeX_2 (X = Cl (**2-Cl$_2$**), Br = (**2-Br$_2$**)) as dark blue-green amorphous solids in acceptable (81%) yields by stirring with the appropriate ferrous halide in THF or *n*-butanol at room temperature and removing the solvent.[26]

Through the course of this work, a more efficient and atom economical synthesis of the iron dihalides was developed in which condensation and metallation were effected in the same reaction vessel. Addition of solid $FeCl_2$ or $FeBr_2$ under a stream of argon gas to a refluxing acetic acid solution of 2,6-dibenzoylpyridine and 2,6-diisopropylaniline resulted in rapid formation of a blue solution. The corresponding dihalides, **2-Cl$_2$** or **2-Br$_2$**, were recovered in high yields (70% or 57%) through removal of solvent, precipitation from CH_2Cl_2 or THF, and subsequent washes with diethyl ether and pentane (Figure 1.2). A related procedure has also been reported by Esteruelas and coworkers, who have obtained similar yields of (^{iPr}PhPDI)$NiCl_2$ when $NiCl_2$ is used as a complexing agent.[29] Although it was discovered that the condensation and metallation of various anilines could be effected in this manner, only the 2,6-diisopropyl aniline derivative was studied for more direct comparison to **1-(N$_2$)$_2$**.

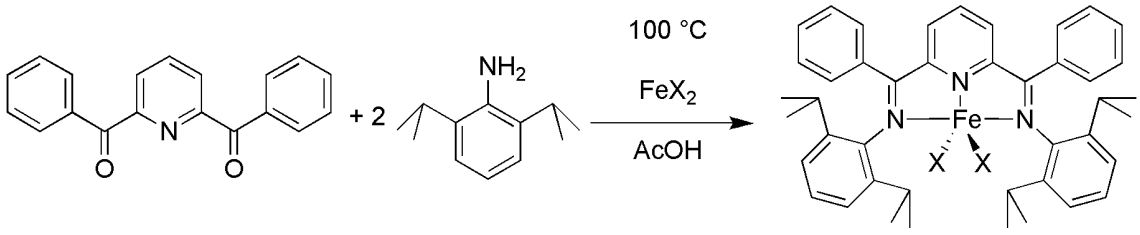

Figure 1.2: Syntheses of dihalides, **2-Cl$_2$** and **2-Br$_2$**.

The ^{1}H NMR spectra of **2-Cl$_2$** and **2-Br$_2$** were acquired in dry, degassed CD_2Cl_2 and C_6D_6, respectively at 22 ºC on a 400 MHz instrument (Figure 1.3). In

analogy to the spectrum of **1-Cl$_2$**,[30] proton resonances are broadened and shifted substantially from values for the free ligand owing to the paramagnetism of the molecules. The resonances for **2-Cl$_2$** and **2-Br$_2$** are spread over ranges of 100 and 120 ppm, respectively with peaks for the *meta*- (77.97 and 74.64 ppm) and *para*-pyridine (82.36 and 101.56 ppm) shifted substantially downfield.

Magnetic susceptibility measurements for **2-Cl$_2$** (5.9 μ_B) and **2-Br$_2$** (5.4) μ_B), which are near that of **1-Cl$_2$** (5.3 μ_B),[30] are characteristic of high-spin, five-coordinate, iron(II) complexes.[31] X-ray diffraction data was not collected on either **2-Cl$_2$** or **2-Br$_2$**, but owing to the C_{2v} symmetry observed by ^{1}H NMR spectroscopy, the molecules are likely to have distorted trigonal-bipyramidal geometries in analogy to **1-Cl$_2$**. [30,32]

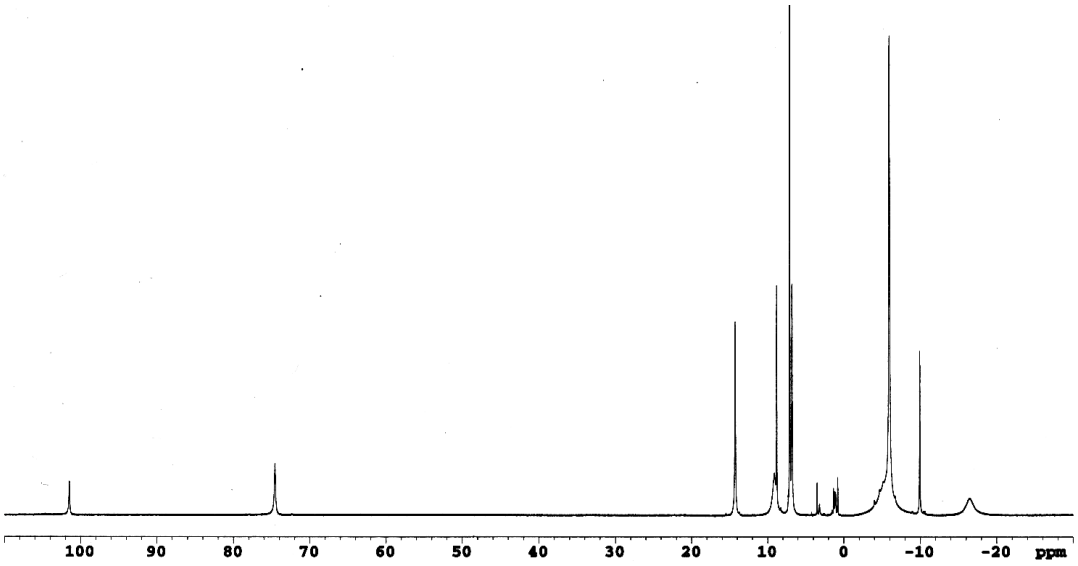

Figure 1.3: ^{1}H NMR spectrum of **2-Br$_2$** recorded at 22 °C in C_6D_6.

Synthesis and Characterization of (^{iPr}PhPDI)Fe(N$_2$)$_2$

Reduction of either **2-Cl$_2$** or **2-Br$_2$** with an excess (~5 equivalents) of 0.5% sodium amalgam under four atmospheres of N_2 afforded the desired iron bis(dinitrogen) complex, (^{iPr}PhPDI)Fe(N_2)$_2$ (**2-(N$_2$)$_2$**) (Figure 1.4), as a brown solid.

Notably, reduction under less than four atmospheres of N_2 led to appreciable formation of an unwanted side product owing to rapid arene coordination (*vide infra*).

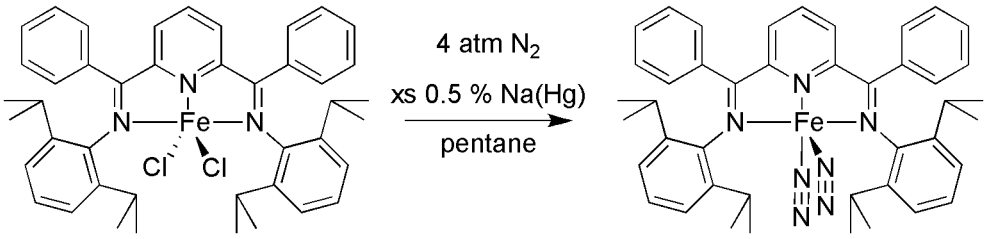

Figure 1.4: Synthesis of the bis(dinitrogen) compound: **2-$(N_2)_2$**.

Single crystals of brown **2-$(N_2)_2$** suitable for X-ray analysis were grown from an ether/pentane solution (1:1) held at –35 °C in the presence of N_2. The solid state structure (Figure 1.5) contained features markedly similar to those of **1-$(N_2)_2$** (Table 1.1). Both molecules exhibit essentially square pyramidal geometries with dinitrogen ligands bound in the apical and basal positions. The dinitrogen ligands in **2-$(N_2)_2$** are similarly unactivated, with N-N bond lengths of 1.106(6) Å (basal) and 1.107(5) Å (apical) near those of free dinitrogen (1.09 Å). The apical dinitrogen ligand of **2-$(N_2)_2$** is slightly bent. The Fe(1)-N(3)-N(4) bond angle of 170.4(5)° is close to that of 171.81(17)° for **1-$(N_2)_2$**. The origin of this distortion is not currently understood.

Bond distances within the structure of **2-$(N_2)_2$** establish two-electron reduction of the bis(imino)pyridine.[33] The C(2)-N(5) and C(8)-N(7) bond lengths, 1.355(7) Å and 1.344(7) Å, are characteristic of C-N single bonds while the C(2)-C(3) and C(7)-C(8) bonds lengths, 1.430(7) Å and 1.429(8) Å, resemble those of C=C double bonds. Values in the structure of **1-$(N_2)_2$** represent similar distortions, indicative of populated molecular orbitals that are antibonding between the C_{imine} and N_{imine} but bonding between C_{ipso} and C_{imine}. Both molecules can thus be formulated as Fe(II) complexed to a bis(imino)pyridine dianion.

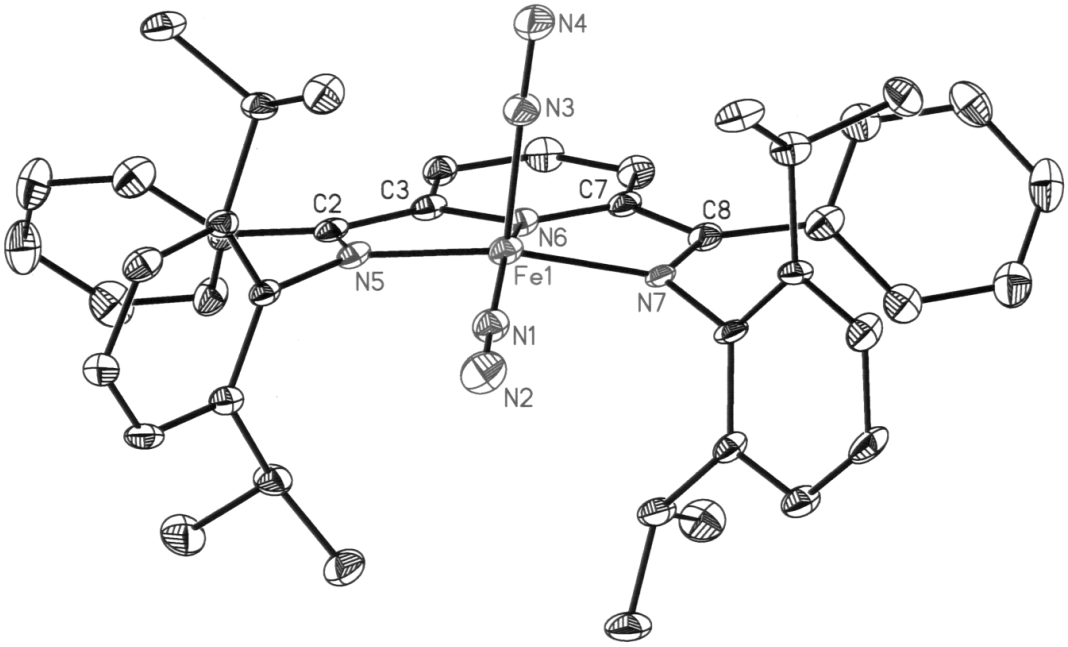

Figure 1.5: Solid state structure of **2-$(N_2)_2$** with 30% probability ellipsoids. Hydrogen atoms omitted for clarity.

Table 1.1: Selected bond distances (Å) and angles (˚) for **1-$(N_2)_2$** and **2-$(N_2)_2$**.

	1-$(N_2)_2$	**2-$(N_2)_2$**
Fe(1)-N(1)	1.8341(16)	1.841(5)
Fe(1)-N(3)	1.8800(19)	1.865(5)
Fe(1)-N(5)	1.9452(16)	1.935(5)
Fe(1)-N(6)	1.8362(14)	1.842(4)
Fe(1)-N(7)	1.9473(16)	1.927(4)
N(1)-N(2)	1.090(2)	1.106(6)
N(3)-N(4)	1.104(3)	1.107(5)
C(2)-N(5)	1.332(2)	1.355(7)
N(6)-C(3)	1.376(2)	1.379(6)
N(6)-C(7)	1.367(2)	1.376(7)
C(8)-N(7)	1.333(2)	1.344(7)
C(2)-C(3)	1.428(3)	1.430(7)
C(7)-C(8)	1.427(2)	1.429(8)
Fe(1)-N(1)-N(2)	178.40(19)	178.5(5)
Fe(1)-N(3)-N(4)	171.81(17)	170.4(5)
N(1)-Fe(1)-N(3)	98.02(8)	99.0(2)
N(1)-Fe(1)-N(5)	96.65(7)	97.2(2)
N(1)-Fe(1)-N(7)	97.41(7)	96.6(2)
N(5)-Fe(1)-N(6)	74.49(6)	80.9(2)
N(6)-Fe(1)-N(7)	79.90(6)	79.3(2)

Surprisingly, the phenyl rings of **2-$(N_2)_2$** are canted at ~45° angles with respect to the pyridine plane. Consequently, there is little overlap between the 2p orbitals of C(1)-C(2) and C(8)-C(9). Thus the phenyl-substituents appear to be out of conjugation with the π-network of the rest of the ligand. An overlay of the two structures (Figure 1.6) highlights another surprising detail. The blade-like alignment of the 2,6-diisopropyl aryl substituents suggests that the increased bulk of the phenyl-substituents has little influence on the steric environment in the binding pocket of **2-$(N_2)_2$**. Together, these observations suggest that the meta-stability of **2-$(N_2)_2$** and the observed differences in catalytic productivity between **2-$(N_2)_2$** and **1-$(N_2)_2$** (*vide infra*) do not precipitate from dissimilar geometries or extended conjugation that might have been endowed by the phenyl substituents.

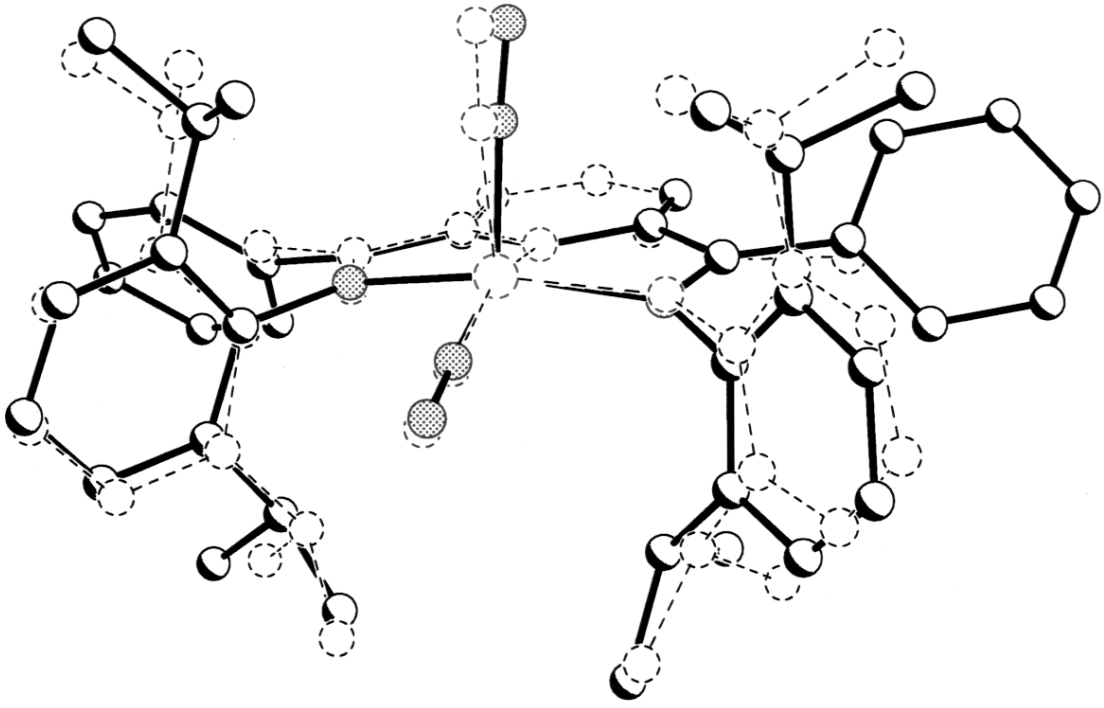

Figure 1.6: Overlay of **1-$(N_2)_2$** (dotted lines) with **2-$(N_2)_2$** (solid lines).

As with **1-$(N_2)_2$**, dinitrogen coordination in **2-$(N_2)_2$** is reversible. Dissolution of **2-$(N_2)_2$** in pentane at 23 °C resulted in the liberation of 1.09 equivalents of non-combustable gas, which was collected by Toepler pump. A second equivalent of N_2 gas was collected after the solution stirred for an additional 48 hours due to the formation of a new product (*vide infra*).

Interconversion of **2-$(N_2)_2$** and **2-N_2** was monitored by in situ infrared spectroscopy. A pentane solution of **2-N_2** at 23 °C displayed a single peak, centered at 2061 cm^{-1}, in the range for dinitrogen bound to bis(imino)pyridine complexes of iron[18]. Upon cooling to -78 °C, this band gradually disappeared with concomitant growth of two intense stretches attributed to **2-$(N_2)_2$** centered at 2086 and 2138 cm^{-1}. At -78 °C the stretch corresponding to **2-N_2** was not observable, suggesting full conversion to **2-$(N_2)_2$** had occurred. Warming the solution back to 23 °C regenerated the band for **2-N_2** concomitant with complete disappearance of bands corresponding to **2-$(N_2)_2$** (Figure 1.7). Notably, solution infrared spectra recorded in benzene at 23 °C displayed a single, intense N-N stretch at 2052 cm^{-1}. Thus, the NMR data recorded in benzene-d_6 at 23 °C is attributed to **2-N_2**.

In spite of the observed paramagnetism (*vide infra*), a sharp, readily assignable ^{1}H NMR spectrum for **2-N_2** was recorded in benzene-d_6 solution (Figure 1.8). The spectrum displays C_{2v} symmetry with resonances for one isopropyl methine and two diastereotopic isopropyl methyl groups. As with **1-N_2**,[18] the resonances for protons in the plane of the iron center, and hence in conjugation with it, are shifted substantially from their diamagnetic free ligand reference values. Far less significant shifts are observed for protons that are removed from the plane of the iron. For example, the para-pyridine proton, which lies in the plane with iron, appears at -0.80 ppm in the complex and at 8.01 ppm in the free ligand. The isopropyl methyl substituents, which

are sufficiently removed from the plane of the iron, appear at –0.71 and 1.16 ppm compared to 1.04 and 1.27 ppm in the free ligand.

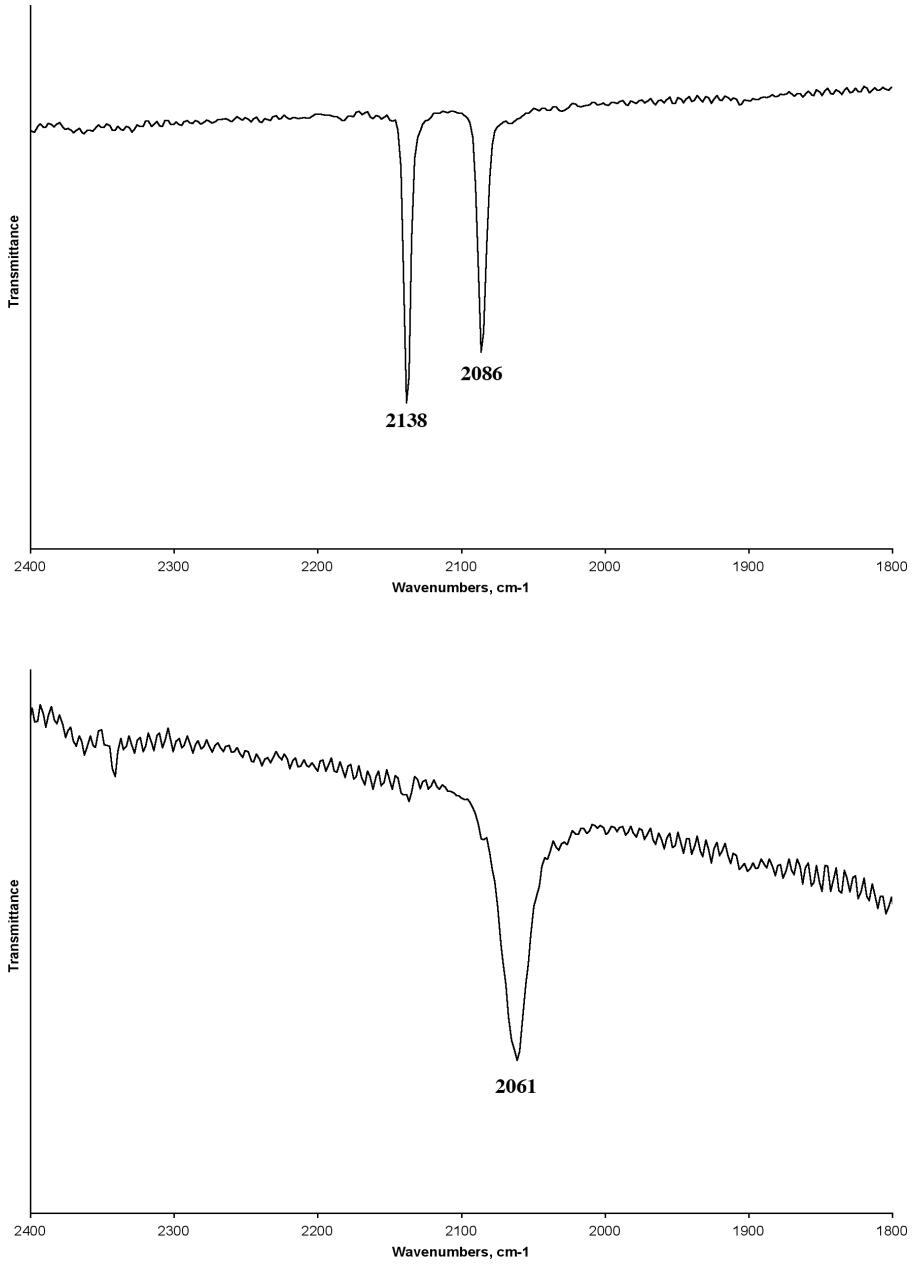

Figure 1.7: Pentane solution infrared spectra of **2-$(N_2)_2$** at –78 °C (top) and **2-N_2** at 23 °C (bottom).

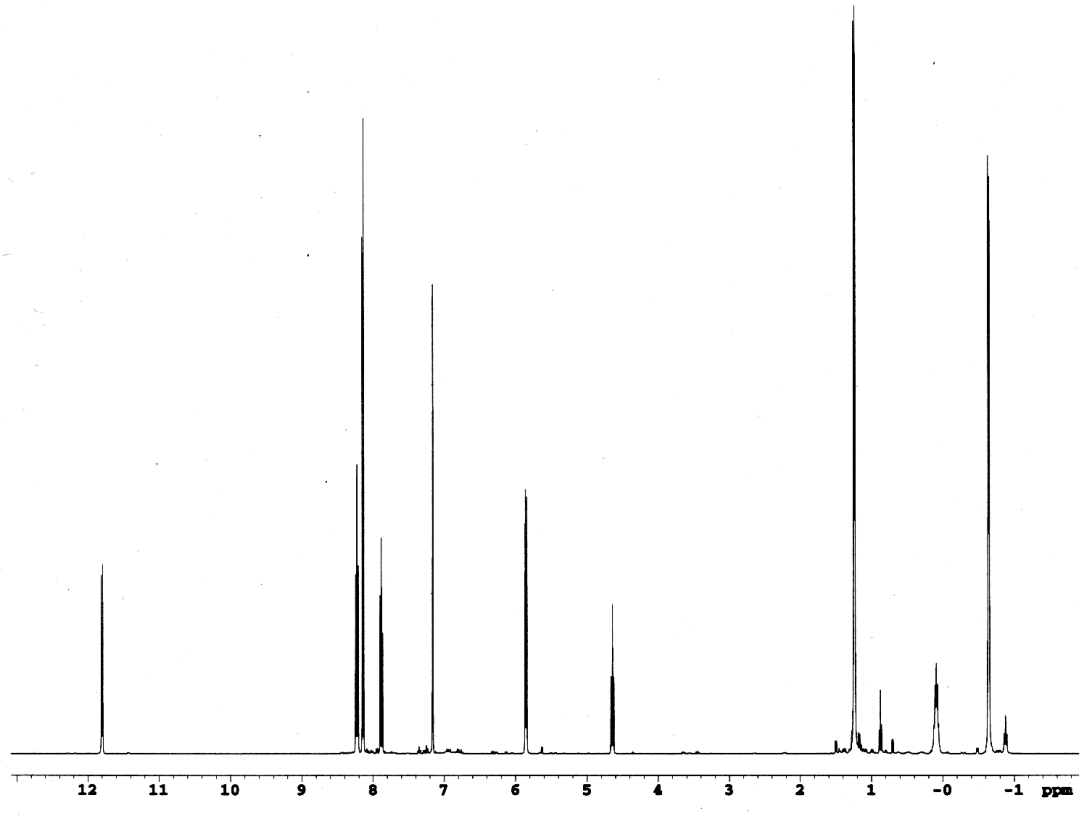

Figure 1.8: ^{1}H NMR spectrum of **2-N_2** recorded at 23 °C in C_6D_6.

Magnetic susceptibility measurements for **2-$(N_2)_2$** differ substantially from those recorded for **1-$(N_2)_2$** and are not straightforward to interpret. Magnetometry data recorded at 23 °C in both the solid state, for **2-$(N_2)_2$** (magnetic susceptibility balance), and in benzene-d_6 solution, for **2-N_2** (Evans Method[34]), independently produced values of μ_{eff} = 1.2(3) μ_B. The observed magnetism is inconsistent with the value reported for **1-$(N_2)_2$** of μ_{eff} = 2.8 μ_B (SQuID), which is characteristic of two unpaired spins on an intermediate spin ferrous center.[18] The purity of **2-$(N_2)_2$** was confirmed by combustion analysis, making it unlikely that the lower measurement could be attributable to contamination with diamagnetic impurities. Instead, the low magnetism suggests substantial contribution from a thermally accessible singlet (S = 0) state.

Comparison of Electronic Properties of (^{iPr}PDI)Fe(N_2)$_2$ and (^{iPr}PhPDI)Fe(N_2)$_2$

To assess changes to the electronic environment afforded by the introduction of phenyl substituents, a systematic comparison of infrared spectroscopy data was sought. The syntheses of (^{iPr}PhPDI)Fe(CO)$_2$ **2-(CO)$_2$** and (^{iPr}PhPDI)Fe(CN^{t}Bu)$_2$ **2-(CN^{t}Bu)$_2$** were undertaken for comparison with **1-(CO)$_2$** and **1-(CN^{t}Bu)$_2$**. Exposure of a solution of **2-N$_2$** to an excess of either carbon monoxide or tert-butylisocyanide followed by solvent removal afforded yellowish-brown solids, which were identified by NMR and IR spectroscopies and by combustion analysis as **2-(CO)$_2$** and **2-(CN^{t}Bu)$_2$**, respectively. Both compounds were more routinely prepared by sodium amalgam reduction of **2-Cl$_2$** in the presence of an excess of either carbon monoxide or tert-butylisocyanide (Figure 1.9).

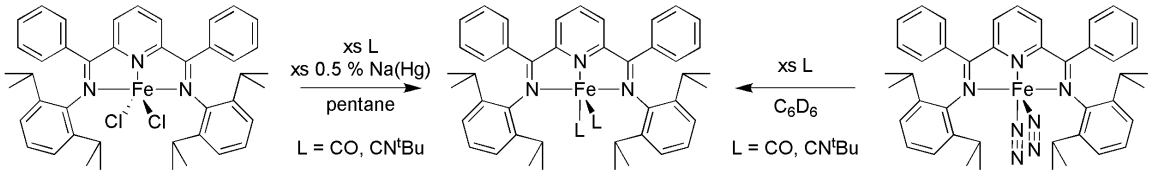

Figure 1.9: Two synthetic routes to **2-(CO)$_2$** and **2-(CN^{t}Bu)$_2$.**

Ambient temperature ^{1}H and ^{13}C NMR spectroscopy of **2-(CO)$_2$** revealed the number of resonances expected for a C_{2v} symmetric molecule, while spectra collected for **2-(CN^{t}Bu)$_2$** displayed the number of resonances for a static C_s symmetric molecule (Figure 1.10). In the ^{1}H NMR spectrum of **2-(CO)$_2$** there are resonances for only two diastereotopic isopropyl methyl groups and one isopropyl methine, while in that of **2-(CN^{t}Bu)$_2$** there are resonances for four diastereotopic isopropyl methyl groups and two distinct isopropyl methines. Two distinct resonances for the tert-butyl methyl groups of the bound isonitriles are also visible. Similar diagnostic NMR features have been observed for **1-(CO)$_2$** and **1-(CN^{t}Bu)$_2$**, where both molecules are pseudo-square

pyramidal but **1-(CO)$_2$** can undergo pseudorotation to equivalence the carbonyl ligands and appear at higher symmetry on the NMR timescale.

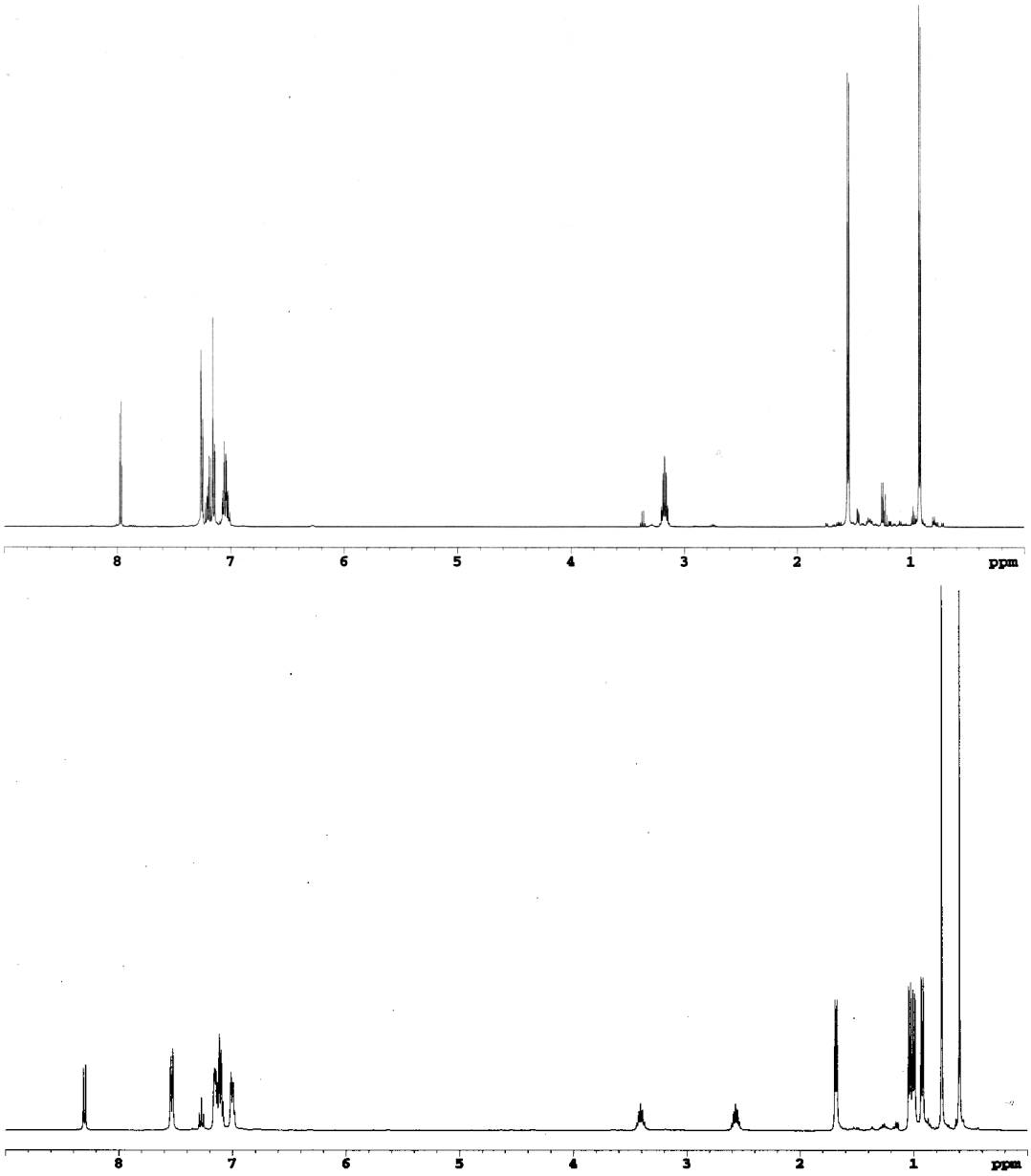

Figure 1.10: ^{1}H NMR spectra of **2-(CO)$_2$** (top) and **2-(CN^{t}Bu)$_2$** (bottom) recorded at 23 °C in C_6D_6.

An indication of the difference in electronic environments for the methyl- versus phenyl- substituted compounds was provided by comparison of infrared

spectroscopic measurements collected for **1-(L)$_n$** and **2-(L)$_n$** (L = N_2, CO, CN^tBu) (n = 1, 2) (Table 1.2).

Table 1.2: IR spectroscopic data for **1-(L)$_n$** and **2-(L)$_n$** (L = N_2, CO, CN^tBu) (n = 1, 2).

	1-(L)$_n$ (cm^{-1})	**2-(L)$_n$** (cm^{-1})
$\nu(N_2)$ (KBr, 23 °C)	2053, 2124	2074, 2130
$\nu(N_2)$ (pentane, -78 °C)	2073, 2132	2086, 2138
$\nu(N_2)$ (pentane, 23 °C)†	2046	2061
ν(CO) (pentane, 23 °C)	1914, 1974	1921, 1979
ν(CN) (pentane, 23 °C)	1976, 2056	1992, 2061

† = (L = N_2) (n = 1)

In all cases, absorptions for complexes with phenyl-substituents appeared at higher values than for methyl-substituted variety. Carbonyl absorptions are shifted to values 5 and 7 cm^{-1} higher in **2-(CO)$_2$** than in **1-(CO)$_2$**. Cyanide bands are elevated by 16 and 5 wavenumbers in **2-(CN^tBu)$_2$** versus **1-(CN^tBu)$_2$**. Also dinitrogen bands consistently appear at higher frequencies in **2-(N_2)$_n$** than in **1-(N_2)$_n$**. Evidently, the iron center of **2-(L)$_n$** is less reducing than that of **1-(L)$_n$**. Although phenyl-substituents are not in conjugation with the π-network of the κ^3-nitrogen moieties in the solid-state (*see above*) σ-inductive effects create an electron-deficient iron center that contributes less electron density into ligand antibonding orbitals through π-backbonds.

To assess electronic differences bestowed on iron centers by the two ligands with a second metric, cyclic voltammetry was performed on **2-(CO)$_2$** for comparison with **1-(CO)$_2$**. As Table 1.3 shows, the compounds display similar electrochemical behaviors; both voltammograms contain one reversible reduction, one reversible oxidation, and one irreversible oxidation. Consistent with its more electron deficient iron center, the features for **2-(CO)$_2$** all occur at subtly higher potentials. Thus, **2-(CO)$_2$** is more easily reduced and more difficult to oxidize than **1-(CO)$_2$**.

Table 1.3: Cyclic voltammetry data for **1-$(CO)_2$** and **2-$(CO)_2$** at 23 °C, .5 mM in THF.

Feature	1-$(CO)_2$ (V)	2-$(CO)_2$ (V)	Δ (2-$(CO)_2$ - 1-$(CO)_2$) (V)
Reversible Reduction	-2.25	-2.21	+0.04
Reversible 1st Oxidation	-0.32	-0.30	+0.02
Irreversible 2nd Oxidation	+0.33	+0.35	+0.02

All values are referenced to ferrocene/ferrocinium and reported relative to Ag/AgCl.

The electronic environments imparted by the methyl- and phenyl-substituted ligands are, thus, subtly different. Phenyl-substituents furnish a more electropositive metal center, which is less easily oxidized and rendered inferior for π-backbonding with ligands and with the π-acidic bis(imino)pyridine terdentate ligand. Because introduction of phenyl rings do not distort the geometry of the molecule significantly, and because the rings are out of conjugation with the π-network of the core of the ligand, this subtle electronic difference must account for the observed differences in reactivity and in catalytic proficiency (*vide infra*).

Catalytic Productivity of 2-$(N_2)_2$ in Olefin Hydrogenation and Hydrosilation

With a second well-defined bis(imino)pyridine iron bis(dinitrogen) complex in hand, differences in catalytic activities could be assessed. The catalytic productivity of **2-$(N_2)_2$** was evaluated for hydrogenation and hydrosilation of olefinic substrates. The hydrogenation reactions were performed on 1.25 M pentane solutions of substrate under 4 atm of $H_{2(g)}$ using 0.3 mol % catalyst. Although lower pressures of H_2 were found to be effective, 4 atm were used to avoid complications from mass transfer effects. Catalytic hydrosilation reactions were also conducted with 1.25 M pentane solutions of substrate at the same, low (0.3 mol %) catalyst loading. Two equivalents of phenyl silane were used for every one equivalent of olefin. Use of less than two equivalents of phenyl silane resulted in formation of detectible quantities of doubly alkylated silanes of the form $PhSiHR_2$.

Three substrates, 1-hexene, cyclohexene, and (R)-(+)-limonene, were selected for an initial assay, the results of which appear in Table 1.4. The progress of each catalytic reaction was monitored by gas chromatography and the reported turnover frequencies were defined either by the time to reach 98 % conversion (for 1-hexene) or by observed conversion after 60 minutes (for cyclohexene and (R)-(+)-limonene). For (R)-(+)-limonene, only the *geminal* olefin was reduced. As with other transition metal-catalyzed hydrosilation reactions,[35] including those catalyzed by **1-$(N_2)_2$**,[18] only anti-Markovnikov addition of the silane was observed.

Table 1.4: Productivities of **1-$(N_2)_2$** & **2-$(N_2)_2$** in catalytic hydrogenation & hydrosilation.

	Hydrogenation T.O.F. (hr^{-1})		**Hydrosilation T.O.F. (hr^{-1})**	
Substrate	**1-$(N_2)_2$**	**2-$(N_2)_2$**	**1-$(N_2)_2$**	**2-$(N_2)_2$**
1-hexene	3300	5300	330	930
cyclohexene	1075	60	20	16
(R)-(+)-limonene	1085	275	166	37

The results of the catalytic study showed that the phenyl-substituted compound was more productive for catalytic hydrogenation and hydrosilation of 1-hexene but was less productive for the more hindered substrates such as cyclohexene and (R)-(+)-limonene. The differences in the relative hydrogenation and hydrosilation productivities of **1-$(N_2)_2$** and **2-$(N_2)_2$** alluded to the existence of a competitive catalyst deactivation pathway for the phenyl-substituted complex. Significantly, no deactivation pathway for **1-$(N_2)_2$** had been observed.

Identification of Catalyst Deactivation Pathways: η^6-Aryl and η^6-Phenyl Bis(imino)pyridine Iron Complexes

To discern whether **2-N_2** was deactivated in solution, the stability of the compound in benzene-d_6 was monitored as a function of time by ^{1}H NMR

spectroscopy. Over the course of hours at 23 ºC, clean and quantitative conversion to two new diamagnetic products in an 85:15 ratio was observed. A combination of multinuclear NMR spectroscopy, combustion analysis, and X-ray diffraction identified the new products as the bis(imino)pyridine iron η^6-phenyl compound, **2-Phenyl** (major, 85 %) and the η^6-2,6-diisopropylphenyl complex, **2-Aryl** (minor, 15 %) (Figure 1.11).

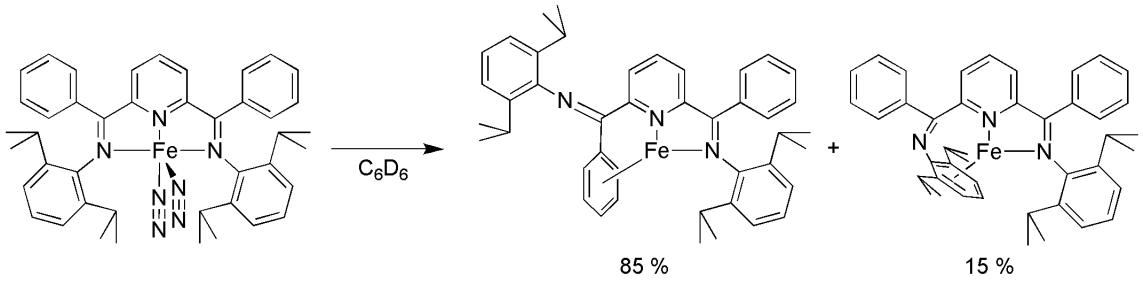

Figure 1.11: 2-$(N_2)_2$ converts cleanly and quantitatively to **2-Phenyl** (85%) and **2-Aryl** (15%) in $\mathbf{C_6D_6}$.

Significantly, conversion to the η^6-arene complexes is irreversible. The two arene compounds do not interconvert in solution. Both are unreactive toward dihydrogen, silanes, olefins, isocyanides, and carbon monoxide, even at high temperatures over substantial periods of time (80 °C for 24 hours). Irreversible formation of these two inert compounds during catalysis would, thus, account for the lower productivities of **2-$(N_2)_2$** with substrates that required longer times to achieve complete conversion.

Both η^6-arene complexes were characterized by X-ray diffraction. The solid state structures for both **2-Phenyl** and **2-Aryl** show idealized C_s symmetry; the mirror planes contain the pyridines and are orthogonal to the remaining four aromatic substituents on each molecule (Figure 1.12). Selected metrical parameters are reported in Table 1.5. In the structure of **2-Phenyl**, one isopropyl group was positionally disordered and was successfully modeled. One arm of the bis(imino)pyridine ligand is

dissociated in both structures yielding the κ^2–N,N coordination mode requisite for η^6-arene complexation (*vide infra*).

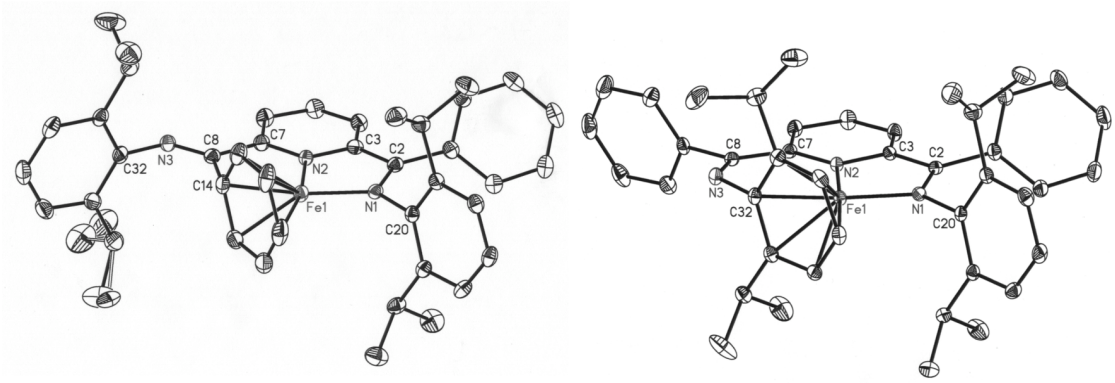

Figure 1.12: Solid state structures of **2-Phenyl** (left) and **2-Aryl** (right) with 30% probability ellipsoids. Hydrogen atoms omitted for clarity.

Table 1.5: Selected bond distances (Å) and angles (˚) for **2-Phenyl** and **2-Aryl.**

	2-Phenyl	**2-Aryl**
Fe(1)-N(1)	1.8956(18)	1.9033(16)
Fe(1)-N(2)	1.8478(18)	1.8798(16)
N(1)-C(2)	1.369(3)	1.351(3)
N(2)-C(3)	1.369(3)	1.405(3)
N(2)-C(7)	1.380(3)	1.391(3)
C(2)-C(3)	1.414(3)	1.419(3)
C(3)-C(4)	1.414(3)	1.401(3)
C(4)-C(5)	1.364(4)	1.362(3)
C(5)-C(6)	1.405(3)	1.405(3)
C(6)-C(7)	1.361(3)	1.378(3)
C(7)-C(8)	1.485(3)	1.483(3)
N(3)-C(8)	1.267(3)	1.283(3)
N(1)-Fe(1)-N(2)	81.36(8)	83.02(7)
C(2)-N(1)-Fe(1)	116.29(15)	116.15(13)
C(3)-C(2)-N(1)	112.08(19)	112.62(17)
C(7)-C(8)-N(3)	120.1(2)	129.72(18)
C(7)-C(8)-C(14)	112.14(19)	112.95(17)

Because one arm of the chelating ligand is dissociated in both compounds, the bond lengths observed on this portion of the ligand are a useful internal reference for unperturbed imine bonds. Consistent with reduction, the N(1)-C(2) bond length in **2-Aryl** elongates to 1.351(3) Å, compared to 1.283(3) Å for the imine on the dissociated arm of the ligand. Similar features are observed in **2-Phenyl** where the N(1)-C(2) bond lengthens to 1.369(3) Å compared to 1.267(3) Å for the imine on the dissociated portion of the ligand. C(2)-C(3) bonds are contracted in the solid state structures for **2-Aryl** and **2-Phenyl** to 1.419(3) and 1.414(3) Å, respectively. Together, these distortions suggest significant contribution from a resonance structure in which there is a single bond between the imine- nitrogen and carbon and a double bond between the imine- and ipso-carbons on the bound arm of the ligand (Figure 1.13). A two electron reduction of the bis(imino)pyridine ligand is implicit in this resonance formulation.[36,37,38,39] Thus, the metrical parameters in conjunction with the observed diamagnetism suggest that a low spin ferrous center is complexed by a κ^2-N,N bis(imino)pyridine dianion.

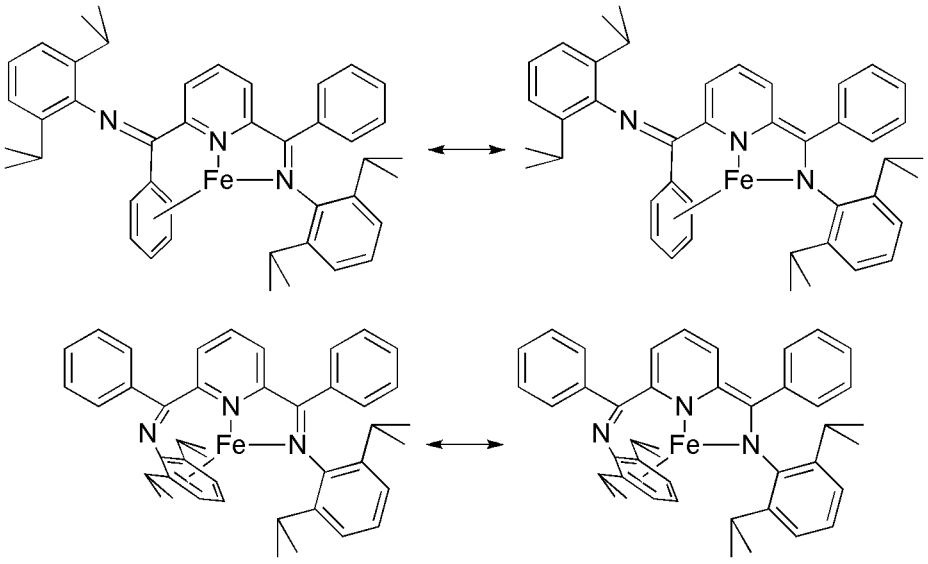

Figure 1.13: Reduction of the bis(imino)pyridine ligands in **2-Phenyl** (top) and **2-Aryl** (bottom).

To confirm the formulation of the ligand as a bis(imino)pyridine dianion, the electronic structure of **2-Aryl** was further investigated with full molecule DFT calculations (ADF2003.01, TZ2P, ZORA). The optimized geometry is in agreement with the experimentally determined solid state structure. The frontier molecular orbitals are presented in Figure 1.14. Notably, the LUMO, which lies 29.8 kcal/mol above the HOMO, is a similar linear combination of ligand orbitals. As has been noted previously, [21,36,37,38,39] the lowest unoccupied molecular orbitals of free aryl-substituted bis(imino)pyridine ligands are π-antibonding with respect to the C_{imine}-N_{imine} bond but π-bonding with respect to C_{ipso}-C_{imine}. Examination of the DFT-computed highest occupied molecular orbital of **2-Aryl** demonstrates this feature and clearly establishes the doubly reduced, dianionic form of the ligand.

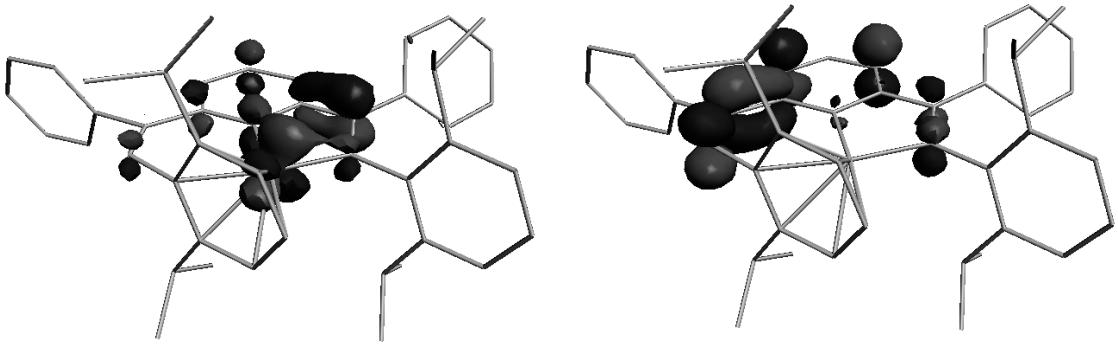

Figure 1.14: DFT computed frontier MO's for **2-Aryl**:
HOMO (left) & LUMO (right).

Our group has previously reported examples of irreversible *intermolecular* η^6-arene complexation to iron in α-diimine compounds.[40] We have also recently observed *intramolecular* η^6-arene coordination during sodium amalgam reduction of alkoxy-substituted bis(imino)pyridine ferrous dibromides.[41] In both cases the chelating ligand is engaged in κ^2–N,N coordination to iron. In the latter case, dissociation of an imine-arm of the terdentate ligand was necessary to achieve this coordination mode,

providing a second example of deleterious bis(imino)pyridine imine lability and irreversible η^6-arene coordination displayed in the deactivation of **2-(N$_2$)$_2$**. Interestingly, the irreversibility of η^6-arene coordination is intrinsic only to iron. Analogous κ^2-N,N bis(imino)pyridine ruthenium η^6-arene complexes rapidly substitute dinitrogen for coordinated arenes at ambient temperature.[42]

Origins of η^6-Arene Coordination.

Because formation of **2-Phenyl** and **2-Aryl** was identified as a major catalyst deactivation pathway for an otherwise effective catalyst, attempts were made to understand the origins of this lamentable reaction. Sealable NMR tubes were charged with equimolar solutions of **2-N$_2$** in benzene-d_6. The headspace in the tubes was either evacuated or contained 1 atm of N_2, 4 atm of N_2, or 4 atm of H_2. Disappearance of **2-N$_2$** was monitored as a function of time by ^{1}H NMR spectroscopy. As Table 1.6 shows, the rate of deactivation was slower at under higher partial pressures of N_2. Pressurizing the headspace of the tube with hydrogen gas did little to inhibit conversion, as the rate of deactivation under 4 atm of $H_{2(g)}$ was only slightly slower than that under vacuum. Significantly, the products consistently appeared in a 5:1 ratio **2-Phenyl**:**2-Aryl**, with no dependence on the identity of the gas in the headspace.

Table 1.6: Effect of gas in the NMR tube headspace on the rate of deactivation of **2-N$_2$** at 23 °C in C_6D_6.

Headspace	Solvent & Temperature	Rate (min^{-1})	Half-life (hr)	Time to 98% conversion (hr)	Product Ratio 2-Phenyl:2-Aryl
Vacuum	C_6D_6 23 °C	1.56×10^{-3}	7.39	41.3	5:1
4 atm H_2	C_6D_6 23 °C	1.18×10^{-3}	9.80	55.4	5:1
1 atm N_2	C_6D_6 23 °C	6.62×10^{-4}	19.2	108	5:1
4 atm N_2	C_6D_6 23 °C	9.27×10^{-5}	125	703	5:1

To test whether the identity of the solvent would affect the products of the reaction, samples of **2-$(N_2)_2$** were dissolved in a range of solvents and stirred under vacuum for 48 hours at 23 °C. After 48 hours, solvents were removed and the residual solids were dissolved in benzene-d_6. ^{1}H NMR spectroscopy was used to identity the products. As Table 1.7 shows, the identity of the solvent had a profound influence on the ratio of products formed. Stirring solutions of **2-N_2** in non-coordinating solvents such as pentane, hexane, diethyl ether, and mesitylene provided exclusive formation of **2-Aryl**.[43] Stirring solutions of **2-N_2** in less-hindered aromatic solvents such as benzene and toluene yielded **2-Phenyl** as the major product (85-90 %) with detectable amounts (10-15 %) of **2-Aryl** present. In more coordinating solvents such as cyclohexene and THF, **2-Phenyl** was observed exclusively. Isolated, purified samples of **2-Phenyl** and **2-Aryl** did not interconvert in solution even when heated to 80 °C for 24 hours. Consequently the observed product ratios are kinetically (rather than thermodynamically) controlled.

Table 1.7: Solvent dependence for the formation of **2-Aryl** versus **2-Phenyl** at 23 °C.

Solvent	% 2-Aryl	% 2-Phenyl
Pentane	100	0
Hexane	100	0
Diethyl Ether	100	0
Mesitylene	100	0
Benzene	15	85
Toluene	10	90
THF	0	100
Cyclohexene	0	100

All experiments stirred under vacuum for 48 hours. **2-N_2** was completely consumed.

Characterization of 2-Aryl and 2-Phenyl

With isolated samples of **2-Aryl** and **2-Phenyl** in hand, characterization of the compounds by NMR spectroscopy and combustion analysis was possible. In benzene-

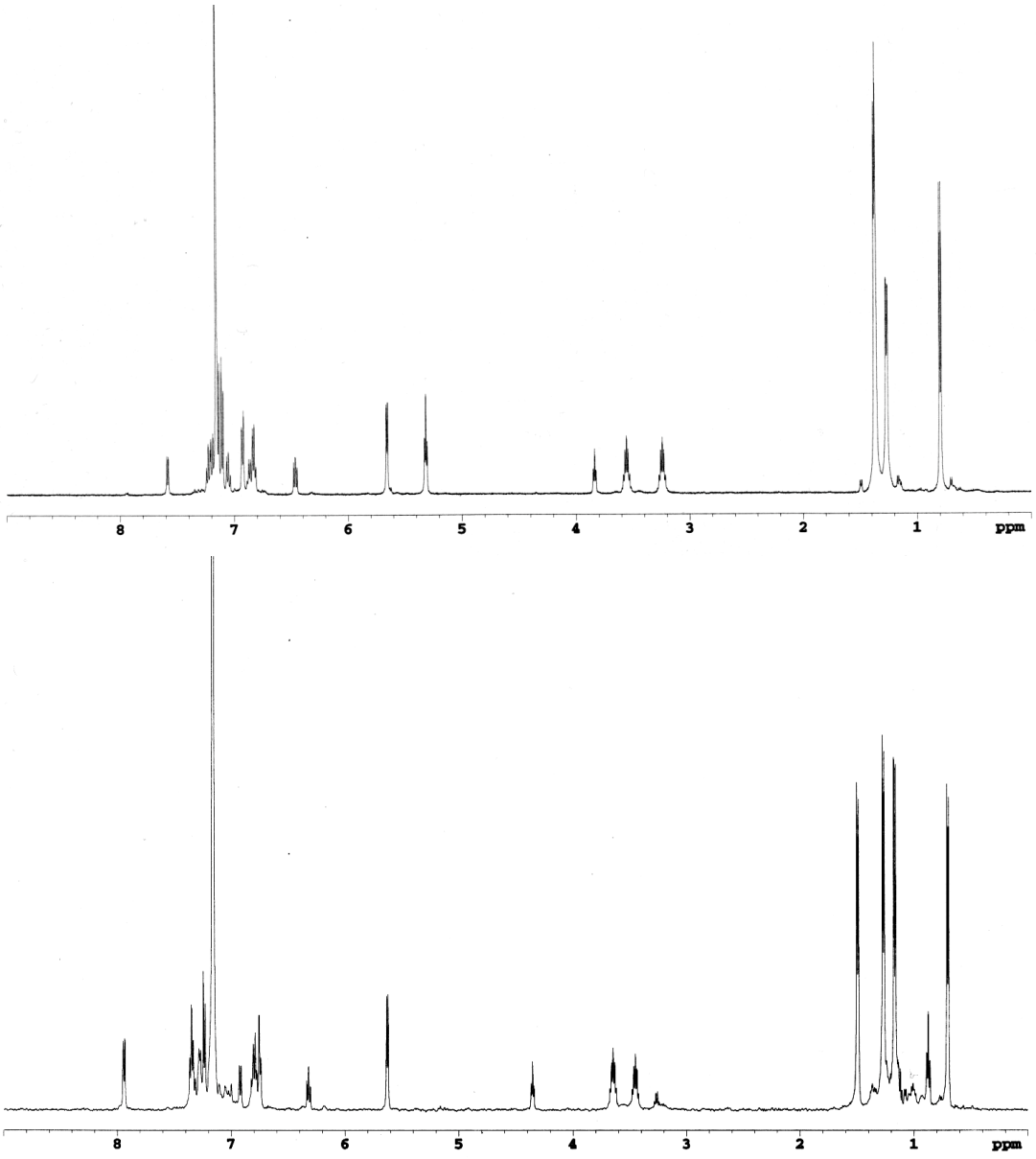

Figure 1.15: ^{1}H NMR spectra of **2-Phenyl** (top) and **2-Aryl** (bottom) recorded at 23 °C in C_6D_6.

d_6 solution, the ^{1}H NMR spectra of both compounds exhibit the number of peaks expected for molecules with C_s symmetry (Figure 1.15). Three upfield shifted aromatic resonances were identified for **2-Phenyl** at 3.85 (*para*-phenyl), 5.32 (*meta*-phenyl) and 5.66 ppm (*ortho*-phenyl), while two were observed for **2-Aryl** at 4.36 (*para*-aryl) and 5.63 ppm (*meta*-aryl). Aromatic proton resonances shifted this far

upfield appear to be the hallmark for iron-bound arenes and have also been observed in spectra for alkoxy-substituted bis(imino)pyridine[41] and α-diimine iron compounds.[40] The ^{1}H and ^{13}C NMR spectra for both compounds were completely assigned with the aid of two-dimensional NMR experiments, and the peak listings are reported in the Experimental Section.

Insight into the Mechanism of η^6-Arene Coordination

Because the formation of the two η^6-arene compounds is irreversible, the product ratio is determined kinetically, rather than thermodynamically. To test whether the two products formed from pathways with competitive relative rates, cyclohexene was titrated into 6.1 mM pentane solutions of **2-N_2**. (Table 1.8) As the concentration of cyclohexene was increased the products included a greater proportion of **2-Phenyl**, although appreciable yields of **2-Aryl** were observed even when 6 equivalents of cyclohexene were present. That both deactivation pathways are accessed argues that the relative rates are competitive.

Table 1.8: Effect of added cyclohexene on ratio of products formed from **2-N_2** at 23 °C in pentane**.**

Equivalents of Cyclohexene Present	% 2-Aryl	% 2-Phenyl
0	100	0
1.0	75	25
2.0	63	37
4.0	47	53

The exclusive formation of **2-Phenyl** in THF was studied for insight into the solvent dependent deactivation mechanism. Dissolution of brown **2-$(N_2)_2$** in THF immediately yielded a purple solution and evolved 1.86 equivalents of non-combustible gas, which was collected by a Toepler pump. Removal of the solvent

yielded a purple solid that was identified based on combustion analysis and NMR spectroscopy as the bis(imino)pyridine iron bis(THF) compound, **2-(THF)$_2$** (Figure 1.16).

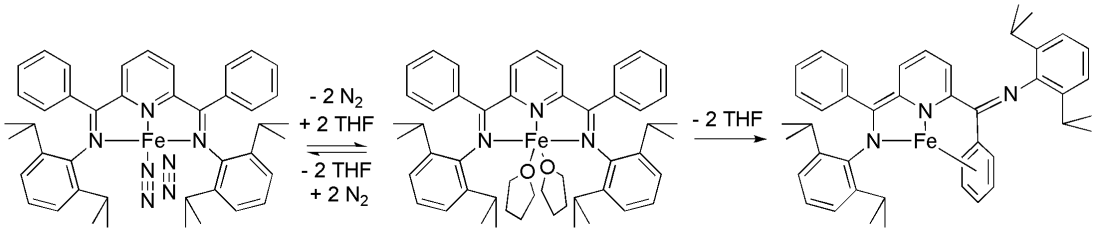

Figure 1.16: Dissolution of **2-(N$_2$)$_2$** in THF permitted isolation of **2-(THF)$_2$**, which converts exclusively to **2-Phenyl** in solvent under vacuum.

Dissolution of solid **2-(THF)$_2$** in solvents such as pentane or in benzene-d_6 under a nitrogen atmosphere immediately liberated two equivalents of THF and regenerated **2-N$_2$**, as determined by ^{1}H NMR spectroscopy. With rigorous exclusion of nitrogen gas, clean samples of **2-(THF)$_2$** could be isolated in benzene-d_6. The ^{1}H NMR spectrum in benzene-d_6 appears in Figure 1.17 and shows the number of resonances expected for a molecule with idealized C_{2v} symmetry. Resonances for protons in the plane of the iron center have the largest isotropic shifts from their diamagnetic reference values. As with **2-(N$_2$)$_2$** the isotropic shifts are attributed to the slight paramagnetism (μ_{eff} = 1.3(1) μ_B) of the molecule. A complete assignment of the ^{1}H and ^{13}C NMR spectra is reported in the Experimental Section.

Permitting benzene-d_6 or THF-d_8 solutions of **2-(THF)$_2$** to stand at 23 °C resulted in quantitative conversion to **2-Phenyl** after 53 and 36 hours, respectively (Figure 1.16). Notably, **2-(THF)$_2$** yielded absolutely no **2-Aryl** as it decayed in benzene-d_6 solution although **2-Aryl** constituted 15% of the product mixture following the decay of **2-N$_2$** in benzene-d_6. Consequently, THF must remain bound throughout

the decay of **2-(THF)$_2$**. Also **2-(THF)$_2$** should be considered a productive intermediate along the pathway toward formation of **2-Phenyl**.

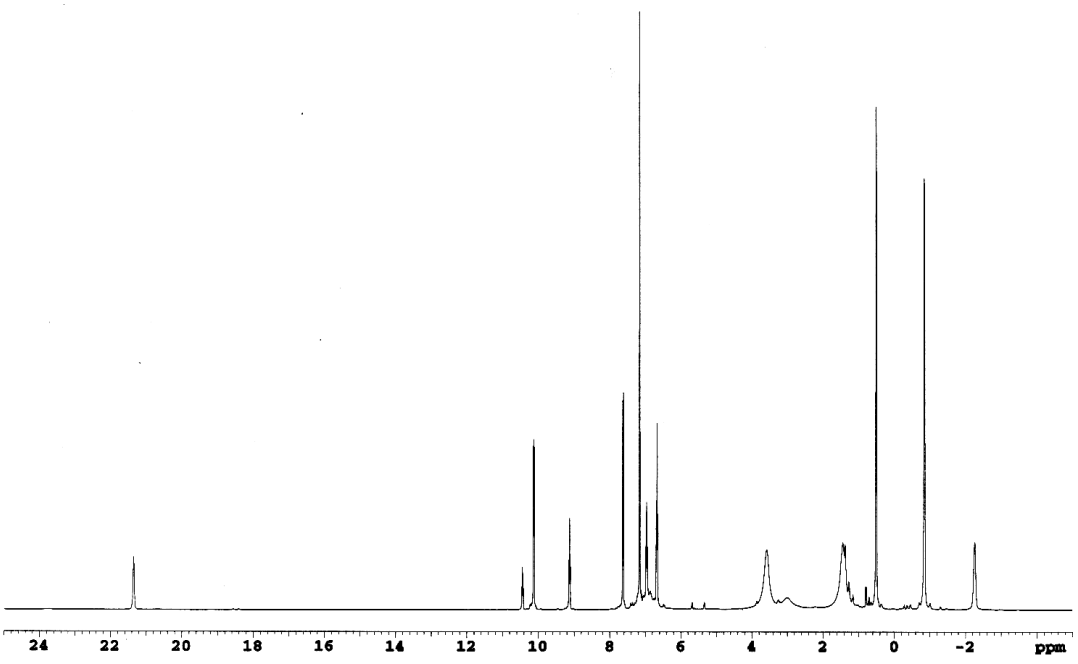

Figure 1.17: ^{1}H NMR spectrum of **2-(THF)$_2$** recorded at 23 °C in C_6D_6.

To determine the reaction order in THF, conversion of **2-(THF)$_2$** to **2-Phenyl** was monitored by ^{1}H NMR spectroscopy in benzene-d_6 a function of THF added. The relative rates were quantified by the time required to reach 98% conversion. As Table 1.9 shows, the presence of excess THF clearly *inhibited* formation of **2-Phenyl**. However, the data suggests that the reaction is not simply inverse first order in THF. Also, observation of a *faster* rate of conversion in neat THF-d_8 suggests a more complex kinetic process is at play, perhaps involving solvation effects.[44]

Table 1.9: Effect of added THF on the relative rate of conversion of **2-(THF)$_2$** to **2-Phenyl** at 23 °C in C_6D_6.

Equivalents of THF Added	Time to Reach 98% Conversion (hr)
0	53
2	69
6	108
25	193
Neat	36

Notably, attempts to isolate the bis(phenylimino)pyridine iron cyclohexene complex were unsuccessful. Dissolution of **2-(N$_2$)$_2$** in neat cyclohexene for five minutes and removal of volatiles afforded a red solid. However, dissolution of this residue in benzene-*d$_6$* under vacuum immediately resulted in 88 % conversion to **2-Phenyl**, as assessed by ^{1}H NMR spectroscopy. The remaining 12 % of the residual material was identified as resuidual **2-N$_2$**. This observation helps explain the low productivity observed for catalytic hydrosilation and hydrogenation of cyclohexene with **2-(N$_2$)$_2$**.

Proposed Mechanism for η^6-Arene Coordination

Based on our observations, a mechanism for **2-(N$_2$)$_2$** deactivation to η^6-arene complexes has been proposed (Figure 1.18). The data definitively establishes that two competitive deactivation pathways are operative. Without coordinating solvent, the pathway to formation of **2-Phenyl** is inaccessible. Solvent coordination, however, clearly kinetically disfavors the pathway to **2-Aryl**. Instead, solvent-ligated complexes (e.g. **2-THF**) follow only the pathway to **2-Phenyl**. The equilibrium between the dinitrogen compound, **2-N$_2$**, and the solvent-ligated compound, **2-(L)$_n$**, therefore determines the ratio of products formed.

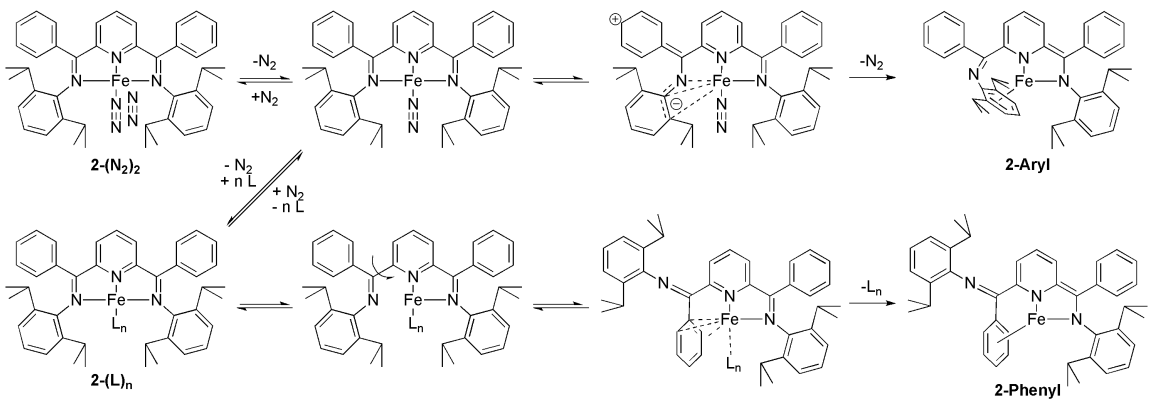

Figure 1.18: Proposed mechanism for the formation of **2-Aryl** (top right) and **2-Phenyl** (bottom right) from **2-$(N_2)_2$**. The product ratio hinges on the equilibrium between **2-N_2** (top, second from left) and **2-$(L)_n$** (bottom left) as the former accesses an aza-aryl intermediate (top, second from right) while the latter proceeds through a κ^2-N,N bis(imino)pyridine intermediate (bottom, second from left).

We propose that the route to **2-Aryl** proceeds through an aza-aryl intermediate. Aza-aryl complexes have been observed for complexes of vanadium[45] and titanium.[46] Presumably, the phenyl-substituents delocalize charge to stabilize the zwitter-ionic aza-aryl resonance form that has subsequent reactivity to form **2-Aryl**. Methyl-substituents would not permit such stabilization and would be unable to access to this deactivation pathway.

To explain the absence of **2-Aryl** formation in coordinating solvent, the activation barrier to formation of the solvent-ligated iron aza-aryl species must be sufficiently large so that the pathway to **2-Aryl** is kinetically disfavored relative to **2-Phenyl**. We propose that the solvent-ligated species, **2-$(L)_n$**, preferentially accesses a κ^2-N,N bis(imino)pyridine iron intermediate. The dinitrogen ligand does not support such an intermediate, but bulkier ligands like THF and cyclohexene do. Dissociation of an imine arm permits rotation about the C_{imine}-C_{ipso} bond and brings the phenyl groups into proximity with the iron center. The phenyl ring then coordinates, displacing solvent. The observation of decreased rate of formation of **2-Phenyl** for **2-$(THF)_2$** with added THF suggests the solvent displacement step would be rate determining.

Implicit in this mechanism is the suggestion that toluene and benzene act as η^2-ligating solvents.[47] Coordination of benzene or toluene must be in the η^2- and not η^6-mode. Otherwise the complexation would be irreversible and would permit observation of these unseen species. Consistent with our proposal, mesitylene solvent does not provide access to the **2-Phenyl** deactivation pathway, perhaps due to its inability to access the η^2-coordination mode

In effort to examine the binding mode of other aromatic solvents, **2-(N_2)$_2$** was treated with N,N-dimethylaminopyridine. Dissolution of brown **2-(N_2)$_2$** in a pentane solution containing one equivalent of N,N-dimethylaminopyridine followed by solvent removal yielded a red solid identified by combustion analysis and multidimensional multinuclear NMR spectroscopy as the corresponding N,N-dimethylaminopyridine compound, **2-(DMAP)** (Figure 1.19). The ^{1}H NMR spectrum of **2-(DMAP)** contains the number of resonances expected for a C_{2v} symmetric molecule, suggestive of an κ^3-N,N,N bis(imino)pyridine ligand with η^2-coordination of the DMAP. Because **2-(DMAP)** proved to be stable in benzene-d_6 solution over the course of days at 23 °C, the DMAP ligand was likely coordinated through the pyridine nitrogen moiety in analogy to crystallographically characterized **1-(DMAP)**.[48]

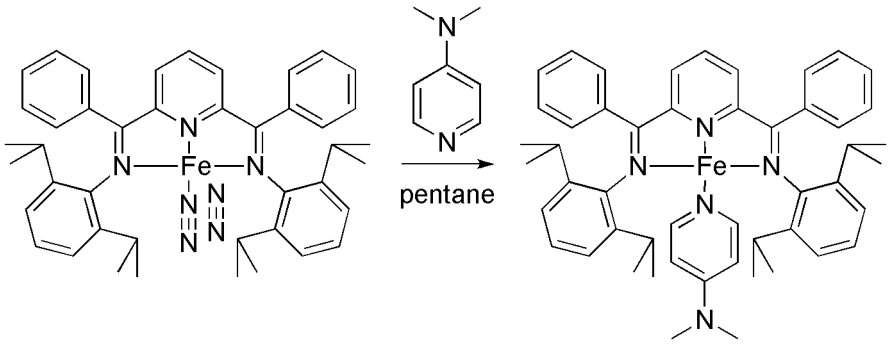

Figure 1.19: Synthesis of **2-(DMAP)**.

1.4 Conclusions

The results presented in this chapter demonstrate how subtle manipulation of the backbone architecture of the bis(imino)pyridine ligand induces irreversible arene coordination to form inert, catalytically inactive complexes. Solvent plays an integral role in determining the selectivity of the products formed. The presence of coordinating solvents is believed to stabilize κ^2-N,N intermediates that facilitate C_{ipso}-C_{imine} bond rotations leading to η^6-phenyl coordination.

1.5 Experimental

General Considerations.

All air- and moisture-sensitive manipulations were carried out using standard vacuum line, Schlenk, and cannula techniques or in an M. Braun inert atmosphere drybox containing an atmosphere of purified nitrogen. The M. Braun drybox was equipped with a cold well designed for freezing samples in liquid nitrogen. Solvents for air- and moisture-sensitive manipulations were initially dried and deoxygenated using literature procedures.[49] Argon and hydrogen gas were purchased from Airgas Inc. and passed through a column containing manganese oxide supported on vermiculite and 4 Å molecular sieves before admission to the high-vacuum line. Benzene-d_6 was purchased from Cambridge Isotope Laboratories, distilled from sodium metal under an atmosphere of argon, and stored over 4 Å molecular sieves or sodium metal. 1-Hexene and cyclohexene were purchased from Acros, dried over $LiAlH_4$, vacuum transferred and filtered through alumina before use. (R)-(+)-Limonene was purchased from Aldrich, dried over $LiAlH_4$, vacuum distilled, and filtered through alumina. Carbon monoxide was purchased from Aldrich and passed through a liquid nitrogen cooled trap immediately before use.

^{1}H NMR spectra were recorded on Varian Mercury 300 and Inova 400 and 500 spectrometers operating at 299.763, 399.780, and 500.62 MHz, respectively. All chemical shifts are reported relative to the peak for $SiMe_4$ using ^{1}H (residual) chemical shifts of the solvent as a secondary standard. For paramagnetic molecules, the ^{1}H NMR data are reported with the chemical shift followed by the peak width at half-height in hertz or multiplicity, the integration value, and, where possible, the peak assignment.

Single crystals suitable for X-ray diffraction were coated with polyisobutylene oil in a drybox and were quickly transferred to the goniometer head of a Siemens SMART CCD area detector system equipped with a molybdenum X-ray tube (_= 0.71073 Å). Preliminary data revealed the crystal system. A hemisphere routine was used for data collection and determination of lattice constants. The space group was identified, and the data were processed using the Bruker SAINT program and corrected for absorption using SADABS. The structures were solved using direct methods (SHELXS) completed by subsequent Fourier synthesis and refined by full-matrix least-squares procedures.

Catalytic reactions were assayed by gas chromatography by comparison to authentic samples. Gas chromatography was performed on a Shimadzu GC-2010 gas chromatograph equipped with an RTX-5 capillary column (15 m) with an injector temperature of 250 °C and a detector temperature of 250 °C. The methods used for separating hydrogenation substrates and products are as follows: cyclohexene/cyclohexane and 1-hexene/*n*-hexane used an oven temperature of 27 °C for 12 min (R)-(+)-limonene/(+)-*p*-menth-1-ene used an oven temperature of 50 °C for 30 min, The methods used for separating hydrosilation substrates and products are as follows: cyclohexene and 1-hexene from the products used an oven temperature of 80 °C for 2 min, with a ramp rate of 10 °C/min to a final temperature of 110 °C for 20

min, (R)-(+)-limonene from the products used an oven temperature of 120 °C for 1 min, with a ramp rate of 20 °C/min to a final temperature of 240 °C for 15 min.

Solution infrared spectra were recorded with an in situ IR spectrometer fitted with a 30-bounce, silicon-tipped probe optimized for sensitivity. The spectra were acquired in 16 scans (30 s intervals) at a gain of 1 and a resolution of 4. A representative reaction was carried out as follows: The IR probe was inserted through a nylon adapter and O-ring seal into a flame-dried, cylindrical flask fitted with a magnetic stir bar and T-joint. The T-joint was capped by a septum for injections and a nitrogen line. Following evacuations under full vacuum and flushing with nitrogen, the flask was charged with toluene and a background was recorded at ambient temperature and at -78 °C. The flask was then charged with a pentane solution of the assayed compound to make the final reaction volume 10.0 mL with approximately 0.005 M concentration. The samples were cooled using an acetone/dry-ice bath. The reactions were recorded between 10 minute intervals.

Cyclic voltammograms (CV's) were collected using 30 mL beakers as electrochemical cells with a 3 mm glassy carbon working electrode, Pt wire as a counter electrode, and Ag wire as a reference in a drybox equipped with electrochemical outlets. CV's were recorded using a Bioanalytical Systems CV-27 voltammograph. All CV's were run at a scan rate of 100 mV/s with a sweep width of ±2 V. Solutions of the individual compounds were prepared by charging a via with 4 mg of compound and 0.400 g (1.03 mmol) of [*n*-Bu_4N][PF_6] and dissolving the solids in 10 mL of THF. This produced solutions of approximately 0.5 mM in compound and 0.1 M in electrolyte. After recording the baseline of a standard 0.1 M solution of electrolyte, CV's were collected for ferrocene and then for the compound. Oxidation potentials were then referenced to the formal potential of ferrocene.

All calculations were performed with the Amsterdam Density Functional Theory (ADF2003.01) suite of programs.[50,51,52] Relativistic effects were included using the zero-order regular approximation. The Vosko, Wilk and Nusair (VWN) local density approximation,[53] Becke's exchange[54] and Perdew's correlation[55] (BP86) were used. The cores of the atoms were frozen up to 1s for C and N and 2p for Fe. Uncontracted Slater-type Orbitals (STOs) of triple z quality with two polarizations were employed. This basis set is denoted TZ2P in the ADF program. Each geometry optimization was carried out without symmetry constraints. Orbital representations were generated using ADF view.

Preparation of (^{iPr}PhPDI)$FeCl_2$ (2-Cl_2): A 500 mL round bottomed flask was charged with 3.560 g (11.67 mmol) of 2,6-dibenzoylpyridine. A solution of 4.149 g (23.40 mmol) of 2,6-diisopropylaniline dissolved in 150 mL of acetic acid and the resulting yellow solution was heated to reflux. Under a stream of argon gas, 1.483 g (11.70 mmol) of $FeCl_2$ was added to the stirring mixture forming a blue slurry. Following the addition, the reflux was resumed for four hours after which time the mixture was cooled to room temperature. Acetic acid from the blue mixture was removed in vacuo on a Schlenk line. Residual solvent was removed under high vacuum. The resulting blue solid was dissolved in a minimal amount of dichloromethane, precipitated by layering with pentane, and recovered on a filter. The filter cake was washed with three 20 mL portions of diethyl ether, three 20 mL portions of pentane and then dried under vacuum yielding 5.96 g (70%) of a dark blue powder identified as **2-Cl_2**. Anal Calcd for $C_{43}H_{47}N_3FeCl_2$: C, 70.50; H, 6.47; N, 5.74. Found C, 70.39; H, 6.75; N, 5.75. Magnetic Susceptibility: μ_{eff} = 5.9 μ_B (solid state balance). ^{1}H NMR (dichloromethane-d_2, 22 ˚C): δ -18.63 (519, 4H, C*H*Me_2), -9.22 (24, 2H, p-Ar), -6.12 (40, 12H, CH*Me*$_2$), 1.41 (d, 88 Hz, 12H, CH*Me*$_2$), 7.07 (190, 2H,

p-Ph), 7.40 (36, 4H, 36, m/o-Ph), 8.08 (21, 4H, m/o-Ph), 14.42 (46, 4H, m-Ar), 77.97 (60, 2H, m-Pyr), 82.36 (40, 1H, p-Pyr).

Preparation of (^{iPr}PhPDI)FeBr$_2$ (2-Br$_2$): This compound was prepared using the method described for **2-Cl$_2$** with 1.270 g (4.49 mmol) of 2,6-dibenzoylpyridine, 1.770 g (9.97 mmol) of 2,6-diisopropylaniline and 0.970 g (4.49 mmol) of $FeBr_2$ yielding 2.093 g (57%) of a dark blue powder identified as **2-Br$_2$**. Anal Calcd for $C_{43}H_{47}N_3FeBr_2$: C, 62.87; H, 5.77; N, 5.12. Found C, 62.69; H, 5.54; N, 5.00. Magnetic Susceptibility: μ_{eff} = 5.4 μ_B (solid state balance). ^{1}H NMR (benzene-*d*$_6$, 22 ºC): δ -16.38 (445, 4H, C*H*Me$_2$), -9.86 (26, 2H, p-Ar), -5.86 (55, 12H, CH*Me$_2$*), -5.44 (303, 12H, CH*Me$_2$*), 6.87 (36, 4H, m/o-Ph), 8.89 (22, 2H, p-Ph), 9.20 (237, 4H, m/o-Ph), 14.35 (40, 4H, m-Ar), 74.64 (74, 2H, m-Pyr), 101.56 (60, 1H, p-Pyr).

Preparation of (^{iPr}PhPDI)Fe(N$_2$)$_2$ (2-(N$_2$)$_2$): A thick walled glass vessel was charged with 44.62 g of mercury, approximately 100 mL of pentane and a magnetic stir bar. Sodium metal (0.224 g, 9.76 mmol, 0.5% by weight) was added to the vessel in small (~ 20 mg) portions. The resulting slurry was stirred for 15 minutes to completely dissolve the metal. After this time, a pentane slurry containing 1.429 g (1.024 mmol) of **2-Cl$_2$** was added to the vessel. The vessel was sealed, cooled to liquid nitrogen temperature, and evacuated on a Schlenk line. At –196 ºC, 1 atm of N_2 was added. The vessel was resealed and warmed to ambient temperature. The resulting reaction mixture was stirred for 24 hours after which time brown solution was decanted from the amalgam. The remaining product was extracted from the amalgam into pentane, filtered through Celite, and the solvent from the combined organic layers was removed in vacuo. The resulting brown solid was recrystallized from pentane at –35 ºC yielding 0.558 g (40%) of **2-(N$_2$)$_2$**. Anal Calcd for $C_{43}H_{47}N_7Fe$: C, 71.96; H, 6.60; N, 13.66.

Found C, 71.98; H, 6.64; N, 13.36. Magnetic susceptibility: μ_{eff} = 1.1(1) μ_B (solid state balance and benzene-d_6, 23 ºC). IR (KBr) ν_{N2}: 2074, 2130 cm^{-1}. IR (pentane, -78 ºC) ν_{N2}: 2086, 2138 cm^{-1}. Characterization of **2-N_2**: IR (pentane, 23 ºC): ν_{N2}: 2061 cm^{-1}. IR (benzene, 23 ºC): ν_{N2} = 2052 cm^{-1}. ^{1}H NMR (benzene-d_6, 23 ºC): δ -0.80 (t, 8 Hz, 1H, p-Pyr), -0.71 (d, 6 Hz, 12H, CHMe_2), 0.05 (sept, 6 Hz, 4H, CHMe$_2$), 1.16 (d, 6 Hz, 12H, CHMe_2), 4.61 (t, 8 Hz, 2H, p-Ph), 5.82 (d, 8 Hz, 4H, o-Ph), 7.80 (t, 8 Hz, 2H, p-Ar), 8.05 (d, 8 Hz, 4H, m-Ar), 8.13 (t, 8 Hz, 4H, m-Ph), 11.80 (d, 8 Hz, 2H, m-Pyr). ^{13}C NMR (benzene-d_6, 22 ºC): δ 24.79 (CHMe_2), 40.27 (CHMe_2), 52.18 (CHMe$_2$), 122.85, 124.80, 125.25, 128.06, 130.51, 144.15, 173.57.

Preparation of (^{iPr}PhPDI)Fe(CO)$_2$ (2-(CO)$_2$): A thick walled glass vessel was charged with 6.245 g of mercury, approximately 10 mL of pentane and a stir bar. Sodium metal (0.031 g, 1.4 mmol) was added to the vessel in small (~ 15 mg) portions. The resulting slurry was stirred for 10 minutes to ensure complete dissolution of the metal. A pentane slurry containing 0.200 g (0.273 mmol) of **2-Cl_2** was added to the flask containing the amalgam. The vessel was sealed, cooled to liquid nitrogen temperature and was evacuated. At this temperature 1 atm of CO was added. The reaction mixture was stirred vigorously for 24 hours. The yellowish-brown solution in the resulting mixture was decanted away from the amalgam. Pentane was used to extract the remaining product from the amalgam and both portions were combined and filtered through Celite to remove NaCl. The filtrate was collected and the solvent was removed in vacuo yielding 0.121 g (62 %) a yellowish-brown solid identified as **2-(CO)$_2$**. Anal Calcd for $C_{45}H_{47}N_3O_2Fe$: C, 75.31; H, 6.60; N, 5.85. Found C, 74.97; H, 7.00; N, 5.98. IR (KBr, 23 ºC) ν_{CO}: 1979, 1921 cm^{-1}. IR (pentane, 23 ºC) ν_{CO}: 1979, 1921 cm^{-1}. ^{1}H NMR (benzene-d_6, 22 ºC): δ 0.92 (d, 7 Hz, 12H, CHMe_2), 1.25 (t, 8 Hz, 1H, p-Pyr), 1.55 (d, 7 Hz, 12H, CHMe_2), 3.18 (spt, 7 Hz, 4H, CHMe$_2$), 7.02-7.27

(16H, Ph & Ar), 7.62 (d, 8 Hz, 2H, m-Pyr). ^{13}C NMR (benzene-d_6, 22 ºC): δ, 24.45 (CH*Me*$_2$), 26.84 (CH*Me*$_2$), 28.93 (*C*HMe$_2$), 121.49, 124.39, 125.69, 127.50, 128.45, 128.90, 131.78, 135.24, 141.11, 148.10, 151.05, 158.68.

Preparation of (^{iPr}PhPDI)Fe(CN^{t}Bu)$_2$ (2-(CN^{t}Bu)$_2$): A thick walled glass vessel was charged with 0.037 g (0.052 mmol) of (^{iPr}PhPDI)Fe(N$_2$)$_2$ dissolved in 10 mL of pentane and a stir bar. The vessel was placed in a liquid nitrogen bath and evacuated on the high vacuum line. An excess (0.155 mmol) of dry tertbutylisocyanide was added via calibrated gas bulb. The vessel was resealed, warmed to ambient temperature, and permitted to stir. After five minutes the solution color became a yellowish-brown. After 4 hours, solvent and excess tertbutylisocyanide were removed en vacuo yielding 0.042 mg (98%) of a brown solid. ^{1}H NMR spectroscopy revealed complete consumption of starting material and coincident formation of a new compound identified as (^{iPr}PhPDI)Fe(CN^{t}Bu)$_2$. Anal Calcd for $C_{53}H_{65}N_5Fe$: C, 76.88; H, 7.91; N, 8.46. Found C, 76.99; H, 7.59; N, 8.54. IR (pentane, 23 °C) ν_{CN}: 1992, 2061 cm^{-1}. ^{1}H NMR (benzene-d_6, 22 ˚C): δ 0.60 (s, 9H, ^{t}Bu), 0.75 (s, 9H, ^{t}Bu), 0.92 (d, 7 Hz, 6H, CH*Me*$_2$), 0.99 (d, 7 Hz, 6H, CH*Me*$_2$), 1.03 (d, 7 Hz, 6H, CH*Me*$_2$), 1.68 (d, 7 Hz, 6H, CH*Me*$_2$), 2.56 (sept, 7 Hz, 2H, C*H*Me$_2$), 3.41 (sept, 7 Hz, 2H, C*H*Me$_2$), 7.01 (t, 7 Hz, 4H, m-Ph), 7.10 (d, 7 Hz, 4H, o-Ar), 7.13-7.17 (m, 4H, p-Ar + p-Ph), 7.27 (t, 8 Hz, 1H, p-Pyr), 7.52 (d, 7 Hz, 4H, m-Ar), 8.29 (d, 8 Hz, 2H, m-pyr). ^{13}C NMR (benzene-d_6, 22 ˚C): δ 23.87 (CH*Me*$_2$), 24.91 (*C*H*Me*$_2$), 26.19 (CH*Me*$_2$), 28.24 (CH*Me*$_2$), 28.84 (*C*HMe$_2$), 30.10 (*C*HMe$_2$), 31.45 (3C, CNC*Me*$_3$), 31.60 (3C, CNC*Me*$_3$), 55.69 (CN*C*Me$_3$), 56.97 (CN*C*Me$_3$), 120.08, 120.38, 123.26, 123.94, 125.46, 126.53, 128.24, 131.56, 138.23, 140.46, 143.06, 148.20 (Ar/Ph/Pyr), 153.78 (*C*=N), 154.76 (*C*=N), 189.16 (*C*NCMe$_3$).

Preparation of 2-Aryl: A 50 mL round bottomed flask was charged with 6.245 g of Hg and approximately 500 mL of pentane. Sodium metal (0.031 g, 1.37 mmol) was added to the flask. The resulting amalgam was stirred for 10 minutes. After this time, a pentane slurry containing 0.200 g (0.273 mmol) of **2-Cl$_2$** was added to the amalgam. The resulting red reaction mixture was stirred vigorously for 72 hours and the solution decanted away from the amalgam. The remaining product was extracted from the amalgam with pentane and the extracts combined and filtered through Celite to remove NaCl. The filtrate was collected and the solvent removed in vacuo to yield 0.130 g (72 %) of a red solid identified as **2-Aryl**. Anal Calcd for $C_{43}H_{47}N_3Fe$: C, 78.05; H, 7.16; N, 6.35. Found C, 77.95; H, 7.43; N, 6.59. ^{1}H NMR (benzene-d_6): δ 0.71 (d, 7 Hz, 6H, CHMe_2*), 1.17 (d, 7 Hz, 6H, CHMe_2), 1.27 (d, 7 Hz, 6H, CHMe_2), 1.49 (d, 7 Hz, 6H, CHMe_2*), 3.45 (spt, 7 Hz, 2H, CHMe$_2$), 3.65 (spt, 7 Hz, 2H, CHMe$_2$*), 4.36 (t, 6 Hz, 1H, p-Ar*), 5.63 (d, 6 Hz, 2H, m-Ar*), 6.32 (dd, 8 Hz & 7 Hz, 1H, p-Pyr), 6.74-6.83 (m, 5H, Ph*), 6.92 (dd, 8 Hz & 1 Hz, 1H, m-Pyr*), 7.03 (d, 7Hz, 2H, o-Ph), 7.25 (t, 7 Hz, 2H, m-Ph), 7.32 (dd, 7 Hz & 1 Hz, 1H, m-Pyr), 7.35 (m, 2H, p-Ar & p-Ph), 7.94 (d, 8 Hz, 2H, m-Ar). ^{13}C NMR (benzene-d_6, 22 ˚C): δ 22.39 (CHMe_2), 23.15 (CHMe_2), 24.10 (CHMe_2*), 25.84 (CHMe_2*), 27.90 (CHMe$_2$*), 28.30 (CHMe$_2$), 79.49 (p-Ar*), 80.34 (m-Ar*), 83.48 (o-Ar*), 109.38 (quaternary-Ar*), 118.59 (p-Pyr), 123.52 (Ph), 126.02 (Ph), 126.11 (Ph), 127.49 (Ph), 128.97 (m-Pyr), 129.46 (m-Ar), 130.42 (Ph), 132.42 (Ph), 135.81, 141.43, 143.88, 144.09, 148.19, 149.37, 153.16, 175.31. * denotes resonances on the portion of the molecule where the arene is coordinated to iron.

Preparation of 2-Phenyl: A J. Young NMR tube was charged with 0.017 g (0.024 mmol) of **2-(N$_2$)$_2$** and approximately 0.5 mL of dry tetrahydrofuran. The tube was immersed in a liquid nitrogen bath and evacuated on the high vacuum line. The

contents were then warmed to ambient temperature and shaken for 48 hours. Solvent was removed in vacuo yielding a red oil. A minimal quantity of pentane was used to extract the oil from the tube and was placed in a 20 mL scintillation vial. The pentane was removed in vacuo affording 0.015 g (94 %) of an orange oil identified as **2-Phenyl**. Crystals suitable for X-ray analysis were grown from a pentane solution at -35 °C. Anal Calcd for $C_{43}H_{47}N_3Fe$: C, 78.05; H, 7.16; N, 6.35. Found C, 77.72; H, 6.85; N, 5.95. ^{1}H NMR (benzene-d_6, 22 ºC): δ 0.80 (d, 7 Hz, 6H, CHMe_2), 1.27 (d, 6H, 7 Hz, CHMe_2), 1.37 (d, 12H, 7 Hz, CHMe_2), 3.26 (spt, 2H, 7 Hz, CHMe$_2$), 3.55 (spt, 7 Hz, 2H, CHMe$_2$), 3.85 (t, 6 Hz, 1H, p-Ph*), 5.32 (t, 6 Hz, 2H, m-Ph*), 5.66 (d, 6 Hz, 2H, o-Ph*), 6.47 (dd, 8 Hz & 7 Hz, 1H, p-Pyr), 6.83 (d, 7 Hz, 2H, o-Ph), 6.87 (t, 7 Hz, 1H, p-Ph), 6.93 (t, 7 Hz, 2H, m-Ph), 7.05 (t, 7 Hz, 1H, p-Ar), 7.11 (d, 7 Hz, 2H, m-Ar), 7.14 (d, 9 Hz, 2H, m-Ar), 7.16-7.25 (m, 2H, p-Ar & m-Pyr), 7.58 (dd, 7 Hz & 1Hz, 1H, m-Pyr). ^{13}C NMR (benzene-d_6, 22 ˚C): δ 22.90 (CHMe$_2$), 24.61 (CHMe_2), 24.88 (CHMe$_2$), 26.59 (CHMe_2), 28.52 (CHMe_2), 29.66 (CHMe_2), 80.27 (p-Ph*), 83.96 (o-Ph*), 85.91 (m-Ph*), 89.71 (quaternary-Ph*), 109.81, 122.89, 123.96, 124.07, 125.45, 126.41, 126.47, 129.03, 129.51, 135.87, 136.50, 142.33, 144.54, 147.47, 149.60, 153.35, 166.72, 167.95. * denotes resonances on the portion of the molecule where the phenyl group is coordinated to iron.

Preparation of (^{iPr}PhPDI)Fe(THF)$_2$ (2-(THF)$_2$): A 20 mL scintillation vial was charged with 0.017 g (0.024 mmol) of **2-(N$_2$)$_2$** and approximately 2 mL of THF. The resulting purple solution was stirred for 5 minutes. The volatiles were removed in vacuo yielding 0.019 g (97 %) purple solid identified as **2-(THF)$_2$**. Anal Calcd for $C_{51}H_{61}N_3O_2Fe$: C, 76.20; H, 7.65; N, 5.23. Found C, 75.87; H, 7.75; N, 4.83. Magnetic susceptibility: μ_{eff} = 1.3(1) μ_B (benzene-d_6, 23 ºC). ^{1}H NMR (THF-d_8, 22 ºC): δ -2.42 (30, 4H, CHMe$_2$), -0.99 (13, 12H, CHMe_2), 0.39 (20, 12H, CHMe_2), 6.67 (26, 4H, m-

Ph), 6.84 (26, 2H, p-Ph), 7.68 (19, 4H, o-Ph), 9.51 (25, 2H, p-Ar), 10.29 (23, 4H, m-Ar), 10.61 (25, 1H, p-Pyr), 22.83 (24, 2H, m-Pyr). ^{2}H NMR (THF-d_8, 22 ºC): δ 1.14 (66, 4D, 2,3-THF), 3.00 (5, 4D, 1,4-THF). ^{13}C NMR (THF-d_8, 22 ºC): δ 14.45 (CHMe_2), 23.28 (CHMe_2), 24.06 (broad, 13 Hz, 2,3-THF), 30.00 (broad, 19 Hz, 1,4-THF), 35.13 (CHMe$_2$), 93.98, 116.17, 119.89, 132.83, 134.51, 140.97. ^{1}H NMR (benzene-d_6, 23 ºC): δ -2.26 (25, 4H, CHMe$_2$), -0.84 (11, 12H, CHMe_2), 0.51 (10, 12H, CHMe_2), 1.44 (69, 8H, 2,3-THF), 3.59 (63, 8H, 1,4-THF), 6.67 (t, 7.7 Hz, 4H, m-Ph), 6.96 (t, 7.7 Hz, 2H, p-Ph), 7.63 (d, 7.6 Hz, 4H, o-Ph), 9.13 (t, 7.6 Hz, 2H, p-Ar), 10.12 (d, 7.6 Hz, 4H, m-Ar), 10.44 (t, 7.6 Hz, 1H, p-Pyr), 21.35 (17, 2H, m-Pyr).

Preparation of (^{iPr}PhPDI)Fe(DMAP) (2-(DMAP)): A 20 mL scintillation vial was charged with 0.041 g (0.057 mmol) of **2-(N_2)$_2$** and 0.007 g (0.057 mmol) of solid N,N-dimethylaminopyridine. ~5 mL of diethyl ether was added and the resulting reddish-purple mixture was permitted to stir for four hours. Solvent was removed en vacuo yielding 0.043 g (96%) of a red solid that was recrystallized from an ether solution at -35 ˚C. Anal Calcd for $C_{50}H_{57}N_5Fe$: C, 76.61; H, 7.33; N, 8.93. Found C, 76.56; H, 6.99; N, 8.88. ^{1}H NMR (benzene-d_6, 22 ˚C): δ -2.52 (21 Hz, 1H, p-Pyr), -0.55 (sept, 6 Hz, 4H, CHMe$_2$), 0.00 (d, 6 Hz, 12H, CHMe_2), 0.85 (d, 6 Hz, 12H, CHMe_2), 2.17 (s, 6H, DMAP-Me_2), 6.15 (d, 6 Hz, 2H, m-DMAP), 6.90 (t, 8 Hz, 4H, m-Ph), 7.07 (d, 8 Hz, 4H, m-Ar), 7.20 (d, 6 Hz, 2H, o-DMAP), 7.73 (t, 8 Hz, 2H, p-Ar), 8.32 (t, 8 Hz, 2H, p-Ph), 8.69 (t, 8 Hz, 1H, p-Pyr), 9.43 (d, 8 Hz, 4H, o-Ph), 13.35 (d, 8 Hz, 2H, m-Pyr). ^{13}C NMR (benzene-d_6, 22 ˚C): δ 23.47 (CHMe_2), 24.42 (CHMe_2), 37.40 (CHMe$_2$), 38.65 (DMAP-Me_2) 102.18, 110.10, 112.03, 112.06, 121.81, 124.18, 125.30, 131.64, 138.08, 150.98, 152.76, 156.61, 163.48, 187.66, 190.25.

1.6 References

[1] Cornils, B.; Herrmann, W. A.; *Applied Homogenous Catalysis with Organometallic Compounds*; VCH: Weinheim, Germany, 1996.

[2] Noyori, R. *Asymmetric Catalysis in Organic Synthesis*; Wiley: New York, 1994.

[3] Grubbs, R. H. *Handbook of Metathesis: Volume 2 – Applications in Organic Synthesis*; Wiley-VCH: Weinheim, Germany, 2003.

[4] Grubbs, R. H.; Tumas, W. *Science* **1989**, *243*, 907.

[5] Sharpless, K. B. *Angew. Chem., Int. Ed.* **2002**, *41*, 2024.

[6] Noyori, R. *Angew. Chem., Int. Ed.* **2002**, *41*, 2002.

[7] Baker, R. T.; Tumas, W. *Science* **1999**, *284*, 1477.

[8] Goldshmidt, V. W. *Geochemistry*; Oxford Press: London, 1958.

[9] Koichi, J. *Acc. Chem. Res.* **1974**, *7*, 351.

[10] Fürstner, A.; Leitner, A.; Méndez, M.; Krause, H. *J. Am. Chem. Soc.* **2002**, *124*, 13856.

[11] Bianchini, C.; Mantovani, G.; Meli, A.; Migliacci, F.; Zanobini, F.; Laschi, F.; Sommazzi, A. *Eur. J. Inorg. Chem.* **2003**, 1620.

[12] Knijnenburg, Q.; Horton, A. D.; Van Der Heijden, H.; Gal, A. W.; Budzelaar, P.; Henricus, M. PCT Int. Appl. WO 2003042131, 2003; 26 pp.

[13] Kismartoni, L. C.; Weitz, E.; Cedeno, D. L. *Organometallics* **2005**, *24*, 4714.

[14] Schroeder, M. A.; Wrighton, M. S. *J. Am. Chem. Soc.* **1976**, *98*, 551.

[15] Schroeder, M. A.; Wrighton, M. S. *J. Organomet. Chem.* **1977**, *128*, 345.

[16] Small, B. L.; Brookhart, M.; Bennett, A. M. A. *J. Am. Chem. Soc.* **1998**, *120*, 4049.

[17] Britovsek, G. J. P.; Gibson, V. C.; Kimberley, B. S.; Maddox, P. J.; McTavish, S. J.; Solan, G. A., White, J. P.; Williams, D. J. *Chem. Commun.* **1998**, 849.

[18] Bart, S. C.; Lobkovsky, E.; Chirik, P. J. *J. Am. Chem. Soc.* **2004**, *126*, 13794.

[19] Enright, D.; Gambarotta, S.; Yap, G. P. A.; Budzelaar, P. H. M. *Angew. Chem., Int. Ed.* **2002**, *41*, 3873.

[20] Ingleson, M. J.; Pink, M.; Caulton, K. G. *J. Am. Chem. Soc.* **2006**, *128*, 4248.

[21] Bart, S. C.; Chlopek, K.; Bill, E.; Bouwkamp, M. W.; Lobkovsky, E.; Neese, F.; Weighardt, K.; Chirik, P. J. *submitted*.

[22] Hansch, C.; Leo, A.; Taft, R. W. *Chem. Rev*. **1991**, *91*, 165.

[23] Bouwkamp, M.; Lobkovsky, E.; Chirik, P. J. *Inorg. Chem*. **2006**, *45*, 2.

[24] Reardon, D.; Aharonian, G.; Gambarotta, S.; Yap, G. P. A. *Organometallics* **2002**, *21*, 786.

[25] Sugiyama, H.; Aharonian, G.; Gambarotta, S.; Yap, G. P. A.; Budzelaar, P. H. M. *J. Am. Chem. Soc*. **2002**, *124*, 12268.

[26] Kleigrewe, N.; Steffen, W.; Blömker, T.; Kehr, G.; Fröhlich, R.; Wibbeling, B.; Erker, G.; Wasilke, J.-C.; Wu, G.; Bazan, G. *J. Am. Chem. Soc*. **2005**, *127*, 13955.

[27] Anderson, N.; Soine, T. O. *J. Am. Pharm. Assoc*. **1950**, *39*, 463.

[28] Jain, S. L.; Bhattacharyya, P.; Milton, H. L.; Slawin, A. M. Z.; Crayston, J. A.; Woollins, J. D. *Dalton Trans*. **2004**, 862.

[29] Esteruelas, M. A.; López, A. M.; Méndez, L.; Oliván, M.; Oñate, E. *Organometallics* **2003**, *22*, 395.

[30] Britovsek, G. J. P.; Bruce, M.; Gibson, V. C.; Kimberley, B. S.; Maddox, P. J.; Mastroianni, S.; McTavish, S. J.; Redshaw, C.; Solan, G. A.; Strömberg, S.; White, A. J. P.; Williams, D. J. *J. Am. Chem. Soc*. **1999**, *121*, 8728.

[31] Morassi, R.; Bertinin, I.; Sacconi, L. *Coord. Chem. Rev*. **1973**, *11*, 343.

[32] Bianchini, C.; Mantovani, G.; Meli, A.; Migliacci, F.; Zanobini, F.; Laschi, F.; Sommazzi, A. *Eur. J. Inorg. Chem*. **2003**, 1620.

[33] Scott, J.; Gambarotta, S.; Korobkov, I.; Budzelaar, P. H. M. Organometallics **2005**, *24*, 6298.

[34] Sur, S. K. *J. Magn. Reson*. **1989**, *82*, 169.

[35] Jardine, F. H. *Prog. Inorg. Chem*. **1981**, *28*, 63.

[36] de Bruin, B.; Bill, E.; Bothe, E.; Weyermüller, T.; Wieghardt, K. *Inorg. Chem*. **2000**, *39*, 2936.

[37] Budzelaar, P. H. M.; de Bruin, B.; Gal, A. W.; Wieghardt, K.; van Lenthe, J. H. *Inorg. Chem*. **2001**, *40*, 4649.

[38] Sugiyama, I.; Korobkov, I.; Gambarotta, S.; Mueller, A.; Budzelaar, P. H. M. *Inorg. Chem.* **2004**, *43*, 5771.

[39] Scott, J.; Gambarotta, S.; Korobkov, I.; Knijnenburg, Q.; de Bruin, B.; Budzelaar, P. H. M. *J. Am. Chem. Soc.* **2005**, *127*, 17204.

[40] Bart, S. C.; Hawrelak, E. J.; Lobkovsky, E.; Chirik, P. J. *Organometallics* **2005**, *24*, 5518.

[41] Archer, A. M.; Bouwkamp, M. W.; Cortez M. P.; Lobkovsky, E.; Chirik, P. J. *Organometallics* **2006**, *submitted.*

[42] Yoo, H.; Carroll, P. J.; Berry, D. H. *J. Am. Chem. Soc.* **2006**, *128*, 6038.

[43] The observation of exclusive formation of **2-Aryl** in stirring pentane solutions explains its appearance as an unwanted side-product in sodium amalgam reductions of **2-Cl$_2$**, which are conducted in pentane.

[44] Attempts were also made to study the deactivation of **2-(N$_2$)$_2$** in 1,4-dimethylhydrofuran. However, mixtures of iron products that were isolated from the resulting purple solution were not readily identifiable.

[45] Ruppa, K. B. P.; Desmangles, N.; Gambarotta, S.; Yap, G.; Rheingold, A. L. *Inorg. Chem.* **1997**, *36*, 1194.

[46] Wanandi, P. W.; Davis, W. M.; Cummins, C. C.; Russell, M. A.; Wilcox, D. E. *J. Am. Chem. Soc.* **1995**, *117*, 2110.

[47] For an example of η^2-coordination in iron chemistry see: Sciarone, T. J. J.; Meetsma, A.; Hessen, B.; Teuben, J. H. *Chem. Commun.* **2002**, 1580.

[48] Bart, S. C.; Lobkovsky, E.; Chirik, P. J. *Unpublished Results*

[49] Pangborn, A. B.; Giardello, M. A.; Grubbs, R. H.; Rosen, R. K.; Timmers, F. J. *Organometallics* **1996**, *15*, 1518.

[50] te Velde, G.; Bickelahaupt, F. M.; van Gisbergen, S. J. A.; Fonseca Guerra, C.; Barends, E. J.; Snijders, J. G.; Zielger, T. *J. Comput. Chem.* **2001**, *22*, 931.

[51] Fonseca Guerra, C.; Snijders, J. G.; te Velde, G.; Baerend E. J. *Theor. Chem. Acc.* **1998**, *99*, 391.

[52] Baerends, E. J.; Autschbach, J. A.; Berces, A.; Bo, C.; Boerrigter, P. M.; Cavallo, L.; Chong, D. P.; Deng, L.; Dickson, R. M.; Ellis, D. E.; Fan, L.; Fischer, T. H.; Guerra Fonseca, C.; van Gisbergen, S. J. A.; Groeneveld, J. A.; Gritsenko, O. V.; Grüning, M.; Harris, F. E.; van den Hoek, P.; Jacobsen, H.; van Kessel, G.; Koostra, F.; van Lenthe, E.; Osinga, V. P.; Patchkovshii, S.; Philipsen, P. H. T.; Post, D.; Pye, C. C.; Ravenek, W.; Ros, P.; Schipper, P. R. T.; Schreckenbach, G.; Snijders, J. G.;

Sola, M.; Swart, M.; Swerhone, D.; te Velde, G.; Vernooijs, P.; Versluis, L.; Visser, O.; van Wezenbeek, E.; Wiesenekker, G.; Wolff, S. K.; Woo, T. K.; Ziegler, T. ADF 2002.03 SCM Theoretical Chemistry, Vrije Universiteit, Amsterdam, The Netherlands, http://www.scm.com/.

[53] Vosko, S. H.; Wilk, L.; Nusair, M. *Can. J. Phys.* **1990**, *58*, 1200.

[54] Becke, A. D. *Phys. Rev.* **1988**, *A38*, 2398.

[55] Perdew, J. P. *Phys. Rev.* **1986**, *B33*, 8822.

Chapter 2

Exploration of Bis(imino)pyridine Ligand Modularity for Catalysis with Iron

2.1 Abstract

A family of bis(imino)pyridine ligands bearing alkylimino-substituents (rather than arylimino-substituents) was synthesized and complexed to ferrous dibromide. Conversion to the corresponding dicarbonyl compounds was affected by sodium amalgam reduction under four atmospheres of carbon monoxide. Electronic studies of these alkylimino-substituted bis(imino)pyridine iron dicarbonyls demonstrated the electron-donating character of the ligands relative to their arylimino-substituted counterparts. Initial attempts to isolate effective precatalysts for C-H bond-forming reactions bearing the alkylimino-substituted bis(imino)pyridine ligand were unsuccessful. However, through the course of these attempts, a new precatalyst bearing the arylimino-substituted ^{Et}PDI ligand (^{Et}PDI = (2,6-(2,6-$Et_2C_6H_3N{=}CMe)_2C_5H_3N$) was isolated by sodium amalgam reduction in the presence of excess 1,3-butadiene. The catalytic productivity of this butadiene complex for hydrogenation of simple olefins was assayed. An induction period was identified, and its origins examined.

2.2 Introduction

Interest in using well-defined iron complexes as substitutes for precious-metal catalysts for bond-forming reactions continues to grow.[1] The field has benefited from the recent introduction of bis(imino)pyridine ligands,[2,3] which show promising ability to exchange electron density with the metal[4] and stabilize iron through its intrinsic one electron redox changes.[5] The redox non-innocence[6,7] and appropriate bulk of the bis(imino)pyridine ligand set have yielded iron species with activity for catalytic

olefin polymerization[8,9] approaching that of heavier transition metal catalysts. Recent research in our lab has shown the bis(imino)pyridine ligand, ^{iPr}PDI (^{iPr}PDI = 2,6-(2,6-$^{i}Pr_2C_6H_3N{=}CMe)_2C_5H_3N$), can support an iron bis(dinitrogen) complex, (^{iPr}PDI)Fe$(N_2)_2$ **1-$(N_2)_2$**, that is a versatile precatalyst for hydrogenation, hydrosilation,[10] and single-component polymerization[11] of unfunctionalized terminal and cis- and geminal disubstituted olefins and dienes. However, the scope of the catalyst does not extend to more-substituted olefins.

Capitalizing on, perhaps, the most outstanding features of the bis(imino)pyridine ligand, its ease of synthesis and the modularity it offers, we sought to change the ligand architecture to broaden the substrate scope and/or improve upon the already-remarkable catalytic activity. As shown in Figure 2.1, the bis(imino)pyridine ligand architecture can be changed quite drastically without difficult synthetic work, and a substantial body of research in recent years has focused on the effects permutations to the ligand structure have on activity in catalytic olefin polymerization.[9,12,13,14,15,16,17]

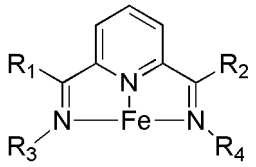

Figure 2.1: The bis(imino)pyridine ligand architecture can easily be altered at positions R_1-R_4.

One portion of this chapter describes the synthesis and characterization of a butadiene complex of iron bearing the ^{Et}PDI (^{Et}PDI = 2,6-(2,6-$Et_2C_6H_3N{=}CMe)_2C_5H_3N$) ligand. The catalytic productivities of two butadiene complexes, ^{Et}PDIFe(η^2,η^2-$CH_2CHCHCH_2$) **3-(Butadiene)** and ^{iPr}PDIFe(η^2,η^2-$CH_2CHCHCH_2$) **1-(Butadiene)**, for hydrogenation of simple olefins were compared. By contrasting the catalytic performances of well-defined species, we hoped to gain

insight into the poorly understood mechanism for catalytic hydrogenation with bis(imino)pyridine complexes of iron. We thought that **3-(Butadiene)**, with one less methyl group on all four sides of its substrate binding pocket, might exhibit productivity and substrate scope exceeding that of **1-(Butadiene)**.

Recently, Bianchini and coworkers have demonstrated that replacement of one of the ligand's arylimino-substituents with an alkylimino-substituent provides a highly active iron dichloride precatalyst for the oligomerization of ethylene.[18] This outcome is particularly exciting, given that chiral primary amines (which afford alkylimino-substituents) are commercially available and are inexpensive, whereas chiral anilines (which afford arylimino-substituted ligands) must be accessed through expensive synthetic routes.[19] Bianchini and coworkers have also recently reported modest enanteomeric excesses in catalytic cyclopropanation with ruthenium complexes supported by bis(imino)pyridine ligands bearing two chiral alkylimino-substituents.[20]

A portion of this chapter also describes the synthesis and characterization of *iron* dibromide and dicarbonyl complexes supported by bis(imino)pyridine ligands bearing two alkylimino-substituents. Activity and control of these complexes for MAO assisted catalytic oligomerization of propylene is currently under investigation.[21]

2.3 Results and Discussion

Synthesis and Characterization of Alkylimino-substituted Bis(imino)pyridine Iron Dibromide Complexes

Synthesis of bis(imino)pyridine ligands bearing two alkylimino-substituents was accomplished using a procedure described in the literature.[20] Condensation of 2,6-diacetylpyridine with the acid sensitive primary amines: diisopropylamine, (R)-(+)-α-methyl-benzylamine, and (R)-(-)-1-cyclohexyl-ethylamine (each 98 % enantiopure),

was affected by stirring neat solutions at 95 °C to yield orange oils of the corresponding ligands **4**, **5**, and **6**.[22] Figure 2.2 displays the ligands discussed in this chapter.

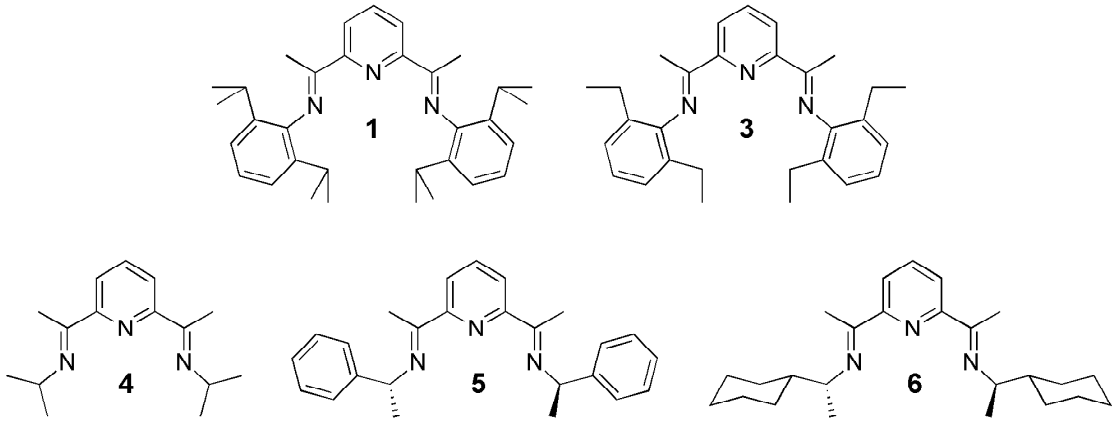

Figure 2.2: Labels in this study for ligands: aryl (**1** and **3**) or alkyl (**4**, **5**, and **6**) bis(imino)pyridines.

The ligands were complexed to iron by stirring with ferrous dibromide in THF at room temperature and removing the solvent. The corresponding iron dibromide complexes, **4-Br$_2$**, **5-Br$_2$**, and **6-Br$_2$**, were isolated in high yields as blue microcrystalline solids. In handling the compounds, it was discovered that all three were far less soluble in toluene than arylimino-substituted complexes (e.g. **1-Br$_2$**).

^{1}H NMR spectra for the compounds were acquired in dry, degassed $CDCl_3$ (**5-Br$_2$**) and CD_2Cl_2 (**4-Br$_2$** and **6-Br$_2$**), respectively, at 22 ºC on a 400 MHz instrument (Figure 2.3). In analogy to the ^{1}H NMR spectrum of **1-Cl$_2$**,[8] the spectra contain the number of peaks expected for C_{2v} (**4-Br$_2$**) or C_2 (**5-Br$_2$** and **6-Br$_2$**) symmetric molecules. Proton resonances appear broadened and shifted substantially from values for the free ligand owing to the paramagnetism (*vide infra*) of the compounds.

The spectra for **4-Br$_2$**, **5-Br$_2$**, and **6-Br$_2$** contain common features, distinguishing the molecules from arylimino-substituted bis(imino)pyridine iron

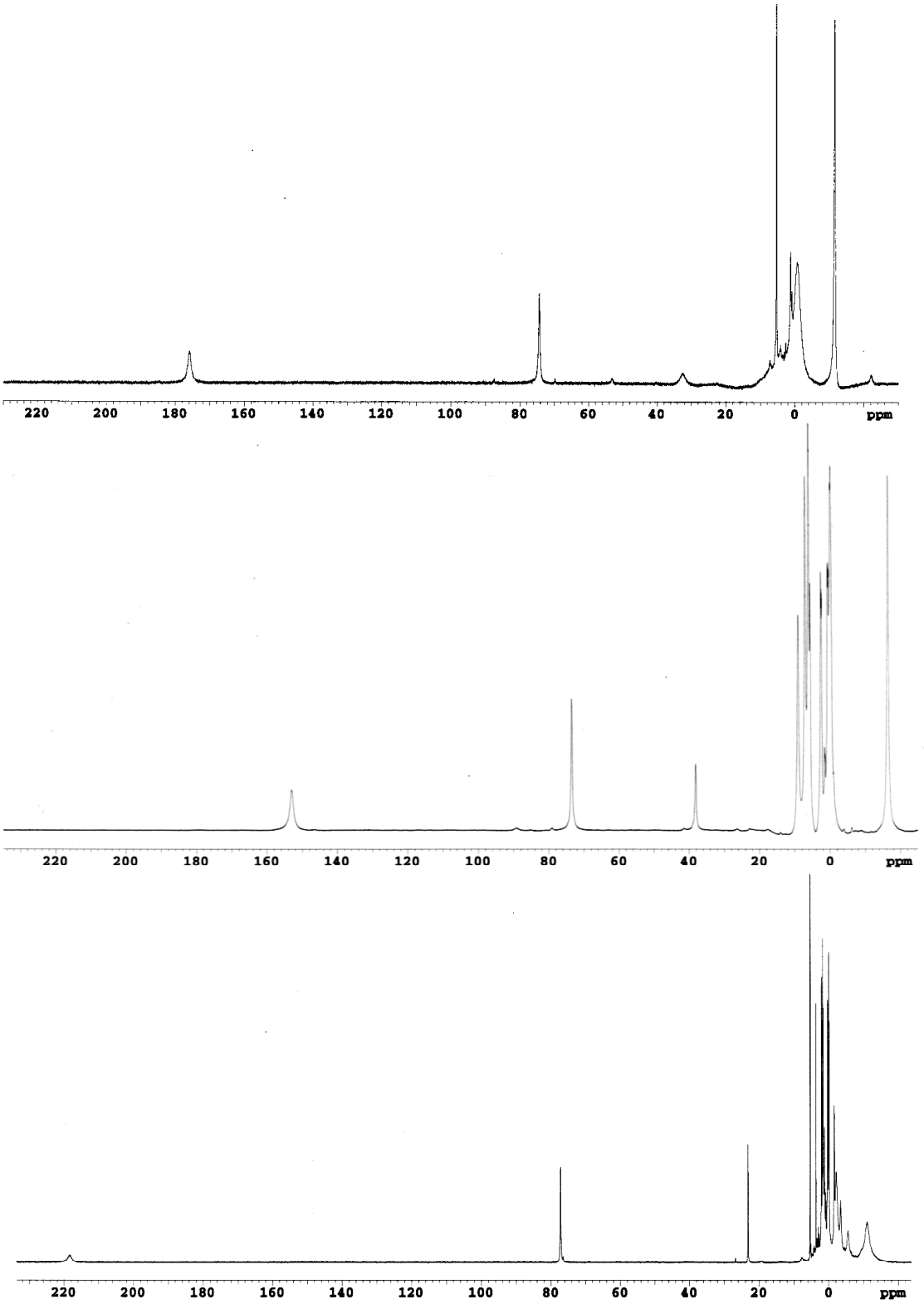

Figure 2.3: ^{1}H NMR spectra of **4-Br$_2$** (top) and **6-Br$_2$** (bottom) recorded at 22 °C in CD_2Cl_2 along with that of **5-Br$_2$** (middle) recorded at 22 °C in $CDCl_3$.

dihalide analogs such as **1-Cl$_2$**. Resonances for the backbone methyl substituents of **4-Br$_2$**, **5-Br$_2$**, and **6-Br$_2$** appear upfield at -11.49, -16.28, and –11.07 ppm, with only modest isotropic shifts from free ligand values (2.31, 2.48, and 2.39 ppm). In **1-Cl$_2$**, the resonance appears at –37.1 ppm, at a much larger isotropic shift from its free ligand value of 2.28 ppm. Also, resonances for the *para*-pyridine protons are shifted only modestly downfield between 20 and 40 ppm (32.46, 38.20, and 23.18 ppm), whereas the resonance appears far downfield at 81.1 ppm for **1-Cl$_2$**. Also, resonances for the *meta*-pyridine protons all appear close to 75 ppm (74.38, 73.57, and 77.21 ppm), slightly upfield of the resonance's location at 81.7 ppm in **1-Cl$_2$**. Finally, resonances in **4-Br$_2$**, **5-Br$_2$**, and **6-Br$_2$** for the imino-bound methine proton, which the arylimino-substituted analogue **1-Cl$_2$** lacks, are located far downfield (176.04, 153.03, and 218.37 ppm), substantially shifted from diamagnetic free ligand values (3.77, 4.95, and 3.49 ppm). These common ^{1}H NMR features are arguably characteristic of the class of alkylimino-substituted bis(imino)pyridine iron dibromide compounds.

Magnetic susceptibility measurements were recorded for all three dibromide complexes using a solid state balance (Table 2.1). The measured values approximate that of **1-Cl$_2$** (5.34 μ_B),[2] and are characteristic of high-spin, five-coordinate, iron(II) complexes.[23] X-ray diffraction data was not collected, but owing to the C_{2v} and C_2 symmetries observed by ^{1}H NMR spectroscopy, the molecules most likely have distorted trigonal-bipyramidal geometries in analogy to **1-Cl$_2$**.[2,18]

Table 2.1: Magnetic Susceptibility Data for **4-Br$_2$**, **5-Br$_2$**, and **6-Br$_2$**.

Compound	μ_{eff} (μ_B)
4-Br$_2$	5.5
5-Br$_2$	5.3
6-Br$_2$	4.9

Comparison of the Electronic Properties of Alkyl Versus Arylimino-substituted Bis(imino)pyridine Iron Complexes

By replacing electron-withdrawing aryl substituents on the ligand with electron donating alkyl substituents, we expected to increase electron density at the iron center.[24] To test our hypothesis and assess changes to the metal's electronic environment, the syntheses of the corresponding dicarbonyl compounds were undertaken. Sodium amalgam reductions of **4-Br$_2$**, **5-Br$_2$**, and **6-Br$_2$** in the presence of 4 atm of carbon monoxide furnished the desired compounds (**4-(CO)$_2$**, **5-(CO)$_2$**, and **6-(CO)$_2$**) as green solids in low, but acceptable yields (Figure 2.4).

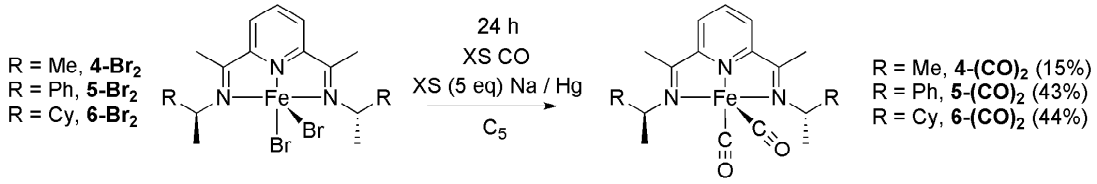

Figure 2.4: Synthesis of dicarbonyls: **4-(CO)$_2$**, **5-(CO)$_2$**, and **6-(CO)$_2$**.

Ambient temperature ^{1}H NMR spectroscopy of the three complexes, performed in benzene-d_6, revealed the number of resonances expected for C_{2v} (**4-(CO)$_2$**) and C_2 (**5-(CO)$_2$** and **6-(CO)$_2$**) symmetric molecules (Figure 2.5). As with **1-(CO)$_2$** the molecules are likely pseudo-square pyramidal but undergo facile pseudorotation to equivalence the carbonyl ligands and appear with higher symmetry on the NMR time scale.[10] The spectra suggest the dicarbonyl compounds are unambiguously diamagnetic. However, resonances in the ^{1}H NMR spectrum of **6-(CO)$_2$** recorded at 20 °C were broad and featureless due to the thermal motion of the cyclohexyl moieties. Cooling the solution to 0 °C provided better resolution.

Collection of pentane solution infrared spectroscopic data for **4-(CO)$_2$**, **5-(CO)$_2$**, and **6-(CO)$_2$** provided a metric to assess changes to the electronic structures provided by alkyl (versus aryl) imino-substituents. As Table 2.2 shows, dicarbonyl

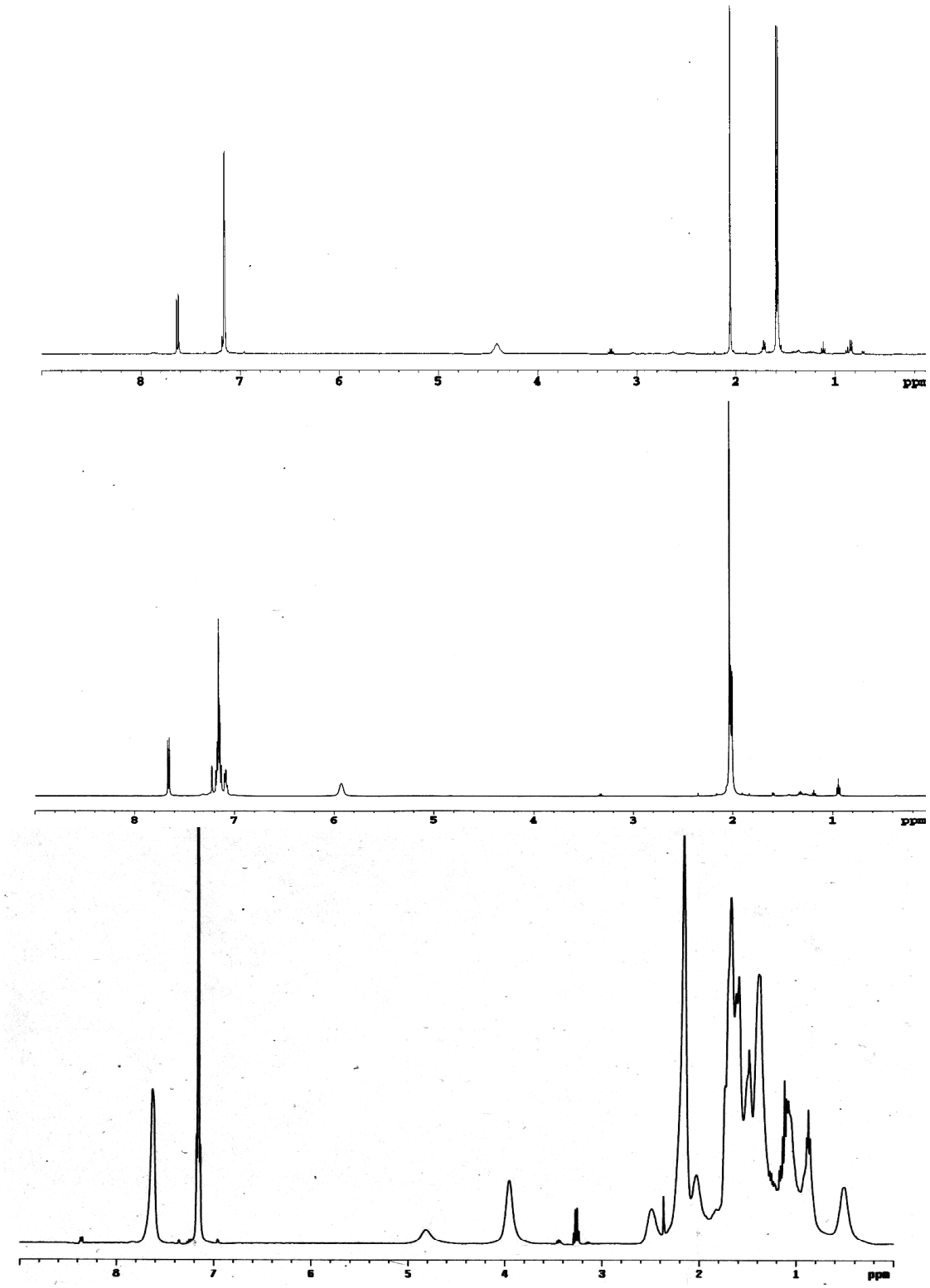

Figure 2.5: ^{1}H NMR spectra for **4-(CO)$_2$** (top), **5-(CO)$_2$** (middle), **6-(CO)$_2$** (bottom) in C_6D_6 at 20 °C.

absorptions appear at markedly lower values for **4-(CO)$_2$**, **5-(CO)$_2$**, and **6-(CO)$_2$** than for **1-(CO)$_2$**. As expected, alkylimino-substituents produce a more electron rich iron center than the arylimino-substituents, so that the iron can contribute more electron density into the antibonding orbitals of the carbonyl ligands through π-backbonding interactions. Curiously, the carbonyl streches for **5-(CO)$_2$** appear at the lowest frequencies suggesting that the methylbenzyl imino-substituted ligand, **5**, is *most reducing* of the class. Hammet principles, however, argue that **5-(CO)$_2$** should be the *least reducing* since the phenyl moiety would be electron-withdrawing relative to either methyl (**4-(CO)$_2$**) or cyclohexyl moieties (**6-(CO)$_2$**).[24]

Table 2.2: Solution IR data for **1-(CO)$_2$**, **4-(CO)$_2$**, **5-(CO)$_2$** and **6-(CO)$_2$**.

	ν_{CO} (cm^{-1})	ν_{CO} (cm^{-1})
1-(CO)$_2$	1914	1974
4-(CO)$_2$	1852	1956
5-(CO)$_2$	1847	1946
6-(CO)$_2$	1889	1953

All spectra recorded at 23 °C in pentane solution.

To shed more light on this discrepancy, cyclic voltammetry was performed in THF at ambient temperature and used as a second metric to assess the relative electronic environments imparted by the ligands. As Table 2.3 shows, **6-(CO)$_2$** had the all of the same redox features as **1-(CO)$_2$** including: one reversible reduction, one reversible oxidation, and one irreversible oxidation. Voltammograms for **4-(CO)$_2$** and **5-(CO)$_2$** showed only the reversible reduction and the reversible oxidation within the assayed sweep-width (-2.95 to 1.05 V relative to Ag/AgCl).

Consistent with their more electron rich iron centers, the reversible reductions of **4-(CO)$_2$**, **5-(CO)$_2$**, and **6-(CO)$_2$** all occur at more negative potentials than **1-(CO)$_2$**. Oxidative behavior follows the same trend on the whole. Reversible oxidations of **4-**

(CO)$_2$ and **5-(CO)$_2$** and the irreversible oxidation of **6-(CO)$_2$** all occur at lower potentials than they do for **1-(CO)$_2$**, demonstrating that higher electron density is present on the iron center. The reversible oxidation of **6-(CO)$_2$**, however, takes place at an anomalously high potential relative to **1-(CO)$_2$**. The origin of this trend-breaking behavior is not currently understood.

Table 2.3: Cyclic voltammetry data for **1-(CO)$_2$, 4-(CO)$_2$, 5-(CO)$_2$,** and **6-(CO)$_2$** at 23 °C, .5 mM in THF.

Feature	1-(CO)$_2$ (V)	4-(CO)$_2$ (V)	5-(CO)$_2$ (V)	6-(CO)$_2$ (V)
Reversible Reduction	-2.25	-2.40	-2.51	-2.43
Reversible 1st Oxidation	-0.32	-0.83	-0.71	-0.09
Irreversible 2nd Oxidation	+0.33			+0.31

All values are referenced to ferrocene/ferrocinium and reported relative to Ag/AgCl.

Consistent with infrared spectroscopy data, **5-(CO)$_2$** appears to have the most negative (most inaccessible) reduction potential. This data confirms that the methylbenzyl imino-substituted ligand, **5**, *is* the most reducing of the class.

Attempts to Isolate Precatalysts for Bond-Forming Reactions

Leaving the reactivity of the alkylimino-substituted bis(imino)pyridine iron dicarbonyl compounds largely unexplored we sought to isolate the corresponding compounds bearing ligands that were more labile than carbon monoxide, which might serve as precatalysts for bond forming reactions. However, reductions of both **4-Br$_2$** and **5-Br$_2$** under a nitrogen atmosphere with either two equivalents of sodium triethylborohydride or an excess (five equivalents) of sodium amalgam yielded intractable mixtures of products.

Reduction of **6-Br$_2$** under identical conditions afforded brown compounds with convoluted, paramagnetic ^{1}H NMR spectra. No infrared absorptions were detected for either product in the region characteristic for bis(imino)pyridine iron dinitrogen

ligands.[10] However, the products of both reductions quickly afforded green **6-(CO)$_2$** along with other diamagnetic material upon exposure to 1 atm of carbon monoxide at 23 °C, as determined by ^{1}H NMR spectroscopy. Consistent with this data, we suggest that a major product in both reductions is the bis(ligand) compound, ($^{(R)MeCy}$APDI)$_2$Fe (*vide infra*) (Figure 2.6).

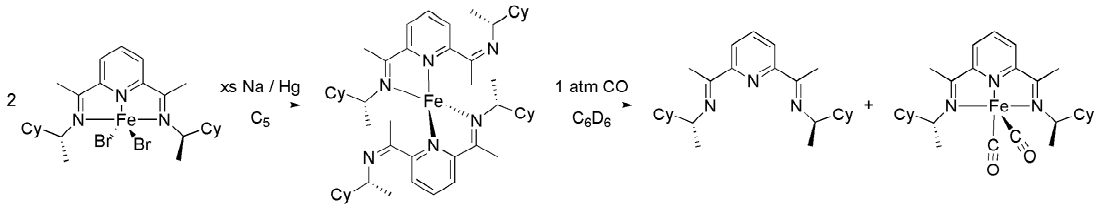

Figure 2.6: Reduction of **6-Br$_2$** (left) yields a brown compound tentatively identified as ($^{(R)MeCy}$APDI)$_2$Fe (middle), which reacts with carbon monoxide at 23 °C to afford **6-(CO)$_2$** (right).

It came as little surprise that alkylimino-substituted bis(imino)pyridine dinitrogen compounds could not be isolated in this manner. Variegated attempts to synthesize stable dinitrogen complexes of iron bearing a bis(methylimino)pyridine ligand other than ^{iPr}PDI have been roundly unsuccessful.[25] Although myriad bis(imino)pyridine iron dihalide complexes are known,[26,27] the conditions[28] and synthetic routes[29] employed to date have been insufficient to evoke coordination of the weak dinitrogen ligand insofar as we have observed. For example, the attempted reductions of (^{Me}PDI)FeCl$_2$, ($^{2,5\text{-}tBu}$PDI)FeBr$_2$, and (PDI)FeCl$_2$ with excesses of sodium amalgam under atmospheric nitrogen yielded brown oils with unintelligable broadened paramagnetic ^{1}H NMR spectra.[30]

A more encouraging "bis(ligand)" product was observed from reduction of (^{Et}PDI)FeCl$_2$ (^{Et}PDI = 2,6-(2,6-Et$_2$C$_6$H$_3$N=CMe)$_2$C$_5$H$_3$N), **3-Cl$_2$**, with sodium amalgam under atmospheric nitrogen.[31] The bis(ligand) compound, (^{Et}PDI)$_2$Fe, presumably forms as two unstable (^{Et}PDI)Fe(0) fragments disproportionate, also precipitating

metallic iron. The $(^{Et}PDI)_2Fe$ complex has been isolated and characterized by X-ray diffraction.[32] In analogy to **2-Phenyl** and **2-Aryl** (See Chapter 1) $(^{Et}PDI)_2Fe$ accesses a κ^2-N,N bis(imino)pyridine coordination mode, further demonstrating the lability of the terdentate ligand. The $(^{Et}PDI)_2Fe$ compound is also relatively inert. It does not catalyze the hydrogenation of 1-hexene and has no reactivity with dinitrogen, hydrogen, or 1,3-butadiene at room temperature. The compound does react with 1 atm of carbon monoxide at 23 °C, however. In analogy to the reactivity displayed by the reduction products of **6-Br$_2$**, treatment of $(^{Et}PDI)_2Fe$ with carbon monoxide affords one equivalent of the corresponding dicarbonyl compound **3-(CO)$_2$** and one equivalent of free ligand (Figure 2.7) as determined by ^{1}H NMR spectroscopy.

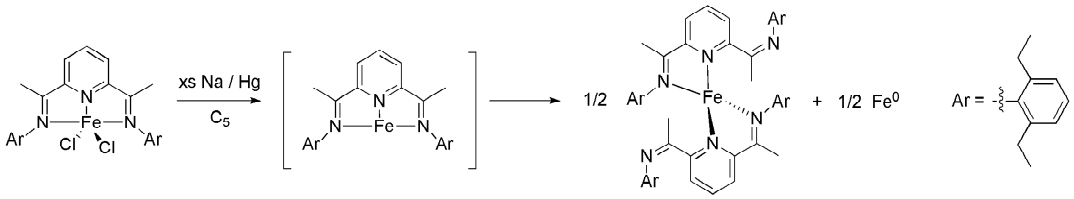

Figure 2.7: Sodium amalgam reduction of **3-Cl$_2$** (left) affords the bis(ligand) compound $(^{Et}PDI)_2Fe$ (right) which likely forms by disproportionation of two iron(0) species (middle).

In attempt to trap the putative bis(imino)pyridine iron(0) fragment and prevent the deleterious disproportionation reaction from transpiring, twenty equivalents of 1,3-butadiene trapping agent were added during reduction with sodium amalgam. Following filtration, a reddish-orange compound was isolated in reasonable (26 %) yield following recrystallization and identified by multidimensional multinuclear NMR spectroscopy and combustion analysis as the corresponding η^2,η^2-1,3-butadiene compound **3-(Butadiene)** (Figure 2.8).

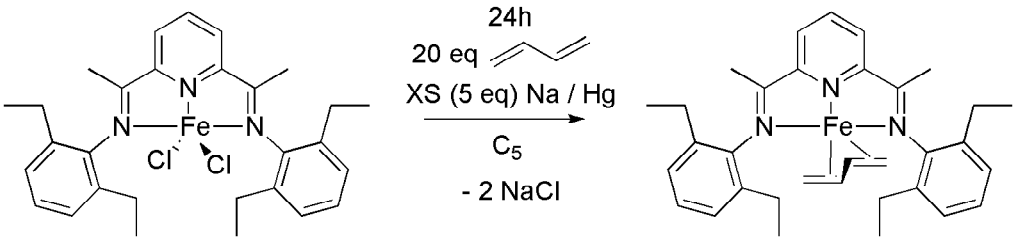

Figure 2.8: Synthesis of the η^2,η^2-butadiene complex: **3-(Butadiene)**.

The ^{1}H NMR spectrum of **3-(Butadiene)** was acquired in benzene-d_6 at 23 °C (Figure 2.9). The spectrum contains number of peaks for a C_s symmetric diamagnetic molecule; there are four resonances for the diastereotopic methylene groups and two resonances for the diastereotopic methyl groups. Also visible are resonances for the η^2,η^2-bound 1,3-butadiene at 2.77, 3.39, and 4.50 ppm. The features evident in the spectrum are much the same as those of (^{iPr}PDI)Fe(η^2,η^2-$CH_2CHCHCH_2$) **1-(Butadiene)**, which our group has previously prepared.[33] The ^{1}H NMR spectrum of **1-(Butadiene)** also reveals the number of resonance for a C_s symmetric diamagnetic compound, with peaks for the η^2,η^2-bound butadiene at 2.95, 3.51, and 4.67 ppm.

The solid-state structure of **1-(Butadiene)** has been determined by X-ray crystallography.[34] The η^2,η^2-butadiene is coordinated in an interesting *trans*-conformation in the solid state, as opposed to the *cis*-conformation observed in the solid state structure of (η^2,η^2-$CH_2CHCHCH_2$)Fe(CO)$_3$.[35,36] As conformational barriers for dienes coordinated to iron are highly influenced by steric factors,[37] it is likely that the narrow binding pocket of the ^{iPr}PDI ligand forces the butadiene into the *trans*-conformation. The smaller Fe-butadiene binding energy in this conformation[38] likely accounts for the ability of **1-(Butadiene)** and **3-(Butadiene)** to catalyze hydrogenation of simple olefins (*vide infra*). Although **3-(Butadiene)** was not crystalographically characterized, a reasonable assumption is that the 1,3-butadiene is coordinated in the same *trans*- conformation or it would not retain the observed catalytic activity.[39]

Frustratingly, attempts to isolate η^2,η^2-butadiene complexes of iron bearing ligands **4**, **5**, and **6** through sodium amalgam reduction in the presence of excess butadiene were unsuccessful. Small yields of oily greenish-brown materials were obtained that showed broad, featureless ^{1}H NMR spectra.

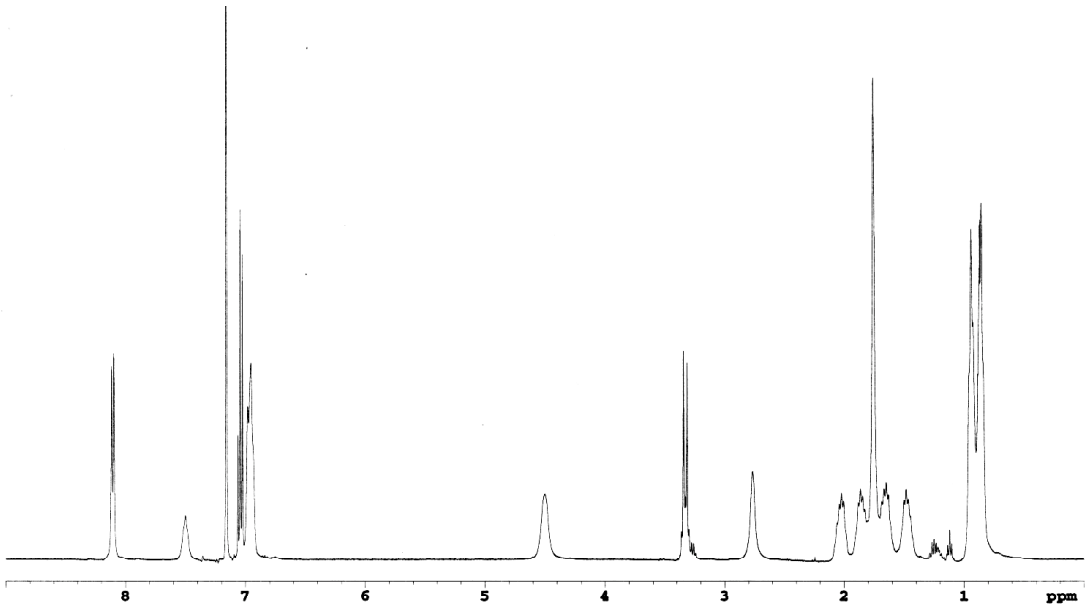

Figure 2.9: ^{1}H NMR spectrum of **3-(Butadiene)** recorded at 20 °C in C_6D_6.

Comparison of the Catalytic Productivities of Two Bis(imino)pyridine Iron Butadiene Complexes

With two similar butadiene complexes in hand, we sought to compare their catalytic productivities. It bears repeating that the mechanism for catalytic hydrogenation observed with **1-(N_2)$_2$** (and also with **1-(Butadiene)**) is not currently known. Thus, it was difficult to predict the effect of modulations of ligand structure would have on the observed catalytic productivities. For instance, if substrate coordination is a rate limiting step in the catalysis, it would be reasonable to assume that **3-(Butadiene)**, with one less methyl group on all four sides of its substrate

binding pocket, would exhibit productivity and substrate scope exceeding that of **1-(Butadiene)**. However, if reductive elimination of alkane is rate limiting, the greater bulk of **1-(Butadiene)** might be an asset, lowering the transition-state energy for reductive elimination event and granting the molecule greater catalytic productivity.

The catalytic productivities of **1-(Butadiene)** and **3-(Butadiene)** were evaluated for hydrogenation of 1-hexene, cyclohexene, and tetramethylethylene. The hydrogenation reactions were performed on 1.25 M pentane solutions of substrate under 4 atm of H_2 using 0.3 mol % catalyst. Although lower pressures of H_2 were found to be effective, 4 atm were used to avoid complications from mass transfer effects. The progress of each catalytic reaction was determined by gas chromatography.

The results of the study showed that both **1-(Butadiene)** and **3-(Butadiene)** served as highly active catalysts for the hydrogenation of 1-hexene, reaching 98% conversion to hexane within 8 minutes (turnover frequencies upwards of 2,500 mol/hr). However, neither catalyst could effect hydrogenation of tetramethylethylene, even after 24 hours, suggesting that the subtle reduction of steric bulk in the binding pocket of **3-(Butadiene)** did little to broaden the substrate scope of the catalyst. Most intriguing was the observation of an induction period in the catalytic hydrogenation of cyclohexene. Cyclohexene persists in solution for 40 minutes with **1-(Butadiene),** or 71 minutes with **3-(Butadiene)**, without being hydrogenated. However, once the catalysts' induction periods have elapsed, hydrogenation proceeds rapidly (Figure 2.10).

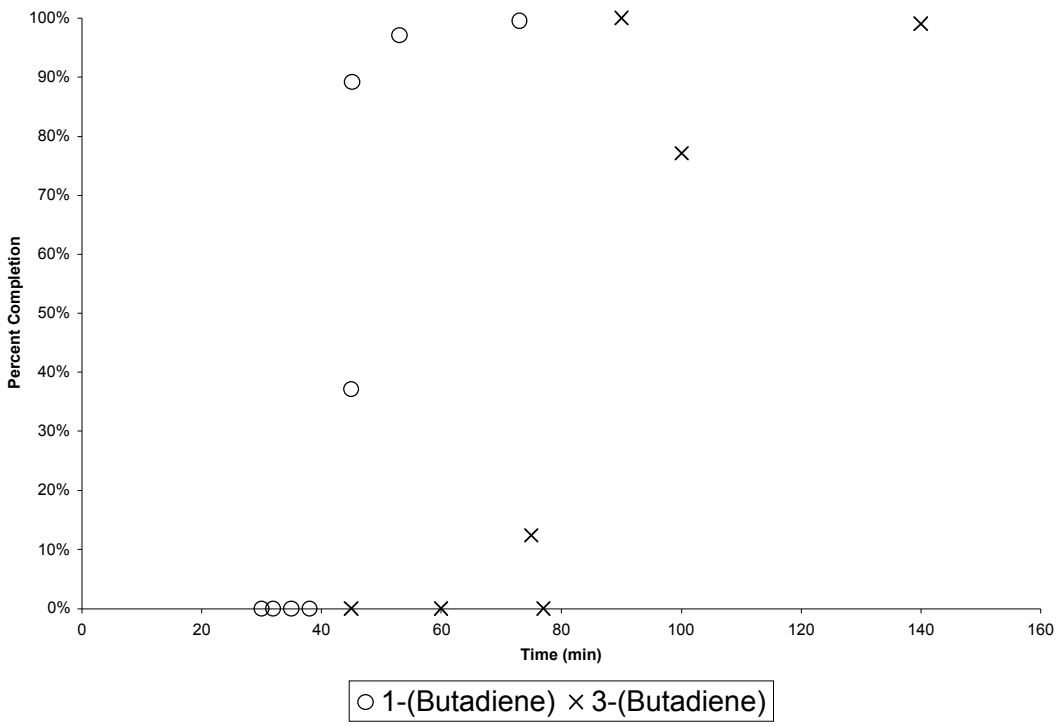

Figure 2.10: Percent of cyclohexene converted to cyclohexane by 0.3 mol % pentane solutions of **1-Butadiene** (circles) or **3-Butadiene** (X's) (as assessed by gas chromatography) is plotted versus time.

Insight into the Observed Induction Period

Induction periods have not been observed in catalysis performed by **1-$(N_2)_2$**.[10] Thus, a logical assumption is that the coordinated butadiene impedes the catalysis of **1-(Butadiene)** and **3-(Butadiene)**, and the induction period represents the time required for the precatalyst to displace the butadiene. This displacement event could proceed by four unique pathways: olefin(s) could substitute for butadiene, the butadiene could be partially hydrogenated to butene and then could substitute with an olefin, butadiene could be fully hydrogenated to butane, or butadiene and olefin could cyclize in a Diels-Alder-type reaction. Different pathways could be operative for dissimilar olefinic substrates. The observation of an induction period with cyclohexene and not with 1-hexene could be explained in this context, provided that the full

hydrogenation of butadiene to butane is relatively slow (since this pathway for butadiene displacement is available regardless of substrate).

To test whether complete hydrogenation of the coordinated butadiene to butane was relatively slow, samples of **1-(Butadiene)** and **3-(Butadiene)**, in benzene-d_6 were placed under 4 atm of hydrogen gas. After 5 minutes, conversion was assessed by ^{1}H NMR spectroscopy. Both butadiene compounds were completely intact and no butane or butene was visible in the spectra. The samples were allowed to stand for 4 hours, over which time the reddish-orange solution of **1-(Butadiene)** turned green (but remained homogenous), and the reddish-orange solution of **3-(Butadiene)** turned black and material began to precipitate from solution. ^{1}H NMR spectra of the volatiles from each sample revealed resonances for butane indicating the full hydrogenation of butadiene had occurred by this time. Incidentally, the iron product of hydrogenation of **1-(Butadiene)** was the dihydrogen complex, **1-(H_2)**, for when a benzene-d_6 solution of this product was exposed a nitrogen atmosphere a clean ^{1}H NMR spectrum for **1-(N_2)$_2$** was visible (Figure 2.11). The ^{1}H NMR spectrum of the iron product resulting from hydrogenation of **3-(Butadiene)** collected in benzene-d_6 displayed a veritable forest of peaks, and further characterization was not attempted.

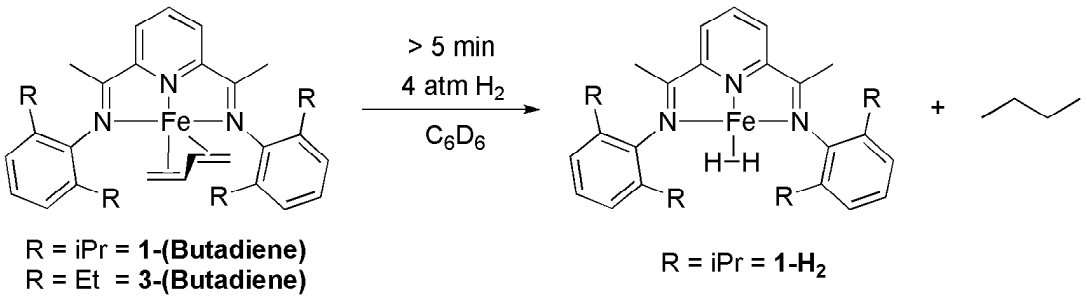

Figure 2.11: At 23 °C in benzene-d_6 solution, **1-(Butadiene)** and **3-(Butadiene)** react *slowly* with hydrogen to afford butane and, in the case of **1-(Butadiene)**, the iron dihydrogen compound, **1-(H_2)**. The identity of the iron product following hydrogenation of **3-(Butadiene)** is not known.

Understanding that two different pathways to butadiene displacement could be operative for 1-hexene and cyclohexene, the reactivity of the butadiene compounds with these olefins in the absence of hydrogen was monitored. Benzene-d_6 solutions of butadiene complexes, **1-(Butadiene)** and **3-(Butadiene)** were permitted to stand under vacuum with an excess (up to 20 equivalents) of either 1-hexene or cyclohexene at 23 °C. Although no conversion of starting material was observed by ^{1}H NMR spectroscopy within 24 hours, resonances in all spectra were noticeably broadened. The broadened features could be the hallmark of dynamic process on the NMR time scale corresponding to rapid on-and-off substitution of olefin for butadiene.

Additional data on the reactivity of **1-(Butadiene)** and **3-(Butadiene)** with olefins and hydrogen would permit us to offer a more sound explanation for the observed induction period. At this point, we propose that both olefins transiently substitute with butadiene in solution. The hydrogenation of 1-hexene is accomplished within the narrow window of time in which it is coordinated to iron. On the other hand, butadiene replaces cyclohexene before the hydrogenation event can occur. Consequently, cyclohexene persists in solution until butadiene is hydrogenated to butane.

2.4 Conclusions

A handful of new alkylimino-substituted bis(imino)pyridine complexes have been synthesized and characterized. Electronic studies clearly show that the alkylimino-substituted bis(imino)pyridine ligands **4**, **5**, and **6** donate greater electron density to the metal center than their arylimino-substituted counterparts (e.g. **1**). The C_2 symmetric dihalide compounds we have synthesized, **5-Br$_2$** and **6-Br$_2$**, are promising precursors to inexpensive iron precatalysts for asymmetric bond-forming reactions.

Following the observation that both **1-(Butadiene)** and **3-(Butadiene)** catalyze hydrogenation of 1-hexene with no induction period, but catalyze hydrogenation of cyclohexene with a substantial induction period, the reactivity of bis(imino)pyridine η^2,η^2-butadiene complexes of iron with olefins and hydrogen gas has been explored. Our findings allude to the intriguing nature of olefin coordination to bis(imino)complexes of iron that warrants further study.

2.5 Experimental

General Considerations.

All air- and moisture-sensitive manipulations were carried out using standard vacuum line, Schlenk, and cannula techniques or in an M. Braun inert atmosphere drybox containing an atmosphere of purified nitrogen. The M. Braun drybox was equipped with a cold well designed for freezing samples in liquid nitrogen. Solvents for air- and moisture-sensitive manipulations were initially dried and deoxygenated using literature procedures.[40] Argon and hydrogen gas were purchased from Airgas Inc. and passed through a column containing manganese oxide supported on vermiculite and 4 Å molecular sieves before admission to the high-vacuum line. Benzene-d_6 and toluene-d_8 were purchased from Cambridge Isotope Laboratories, distilled from sodium metal under an atmosphere of argon, and stored over 4 Å molecular sieves or sodium metal. 1-Hexene, cyclohexene, and tetramethylethylene were purchased from Acros, dried over $LiAlH_4$, vacuum transferred and filtered through alumina before use. Carbon monoxide was purchased from Aldrich and passed through a liquid nitrogen cooled trap immediately before use.

^{1}H NMR spectra were recorded on Varian Mercury 300 and Inova 400 and 500 spectrometers operating at 299.763, 399.780, and 500.62 MHz, respectively. All chemical shifts are reported relative to the peak for $SiMe_4$ using ^{1}H (residual) chemical

shifts of the solvent as a secondary standard. For paramagnetic molecules, the ^{1}H NMR data are reported with the chemical shift followed by the peak width at half-height in hertz or multiplicity, the integration value, and, where possible, the peak assignment.

Catalytic reactions were assayed by gas chromatography by comparison to authentic samples. Gas chromatography was performed on a Shimadzu GC-2010 gas chromatograph equipped with an RTX-5 capillary column (15 m) with an injector temperature of 250 °C and a detector temperature of 250 °C. An oven temperature of 27 °C was used for 12 min to separate hydrogenation substrates and products.

Cyclic voltammograms (CV's) were collected using 30 mL beakers as electrochemical cells with a 3 mm glassy carbon working electrode, Pt wire as a counter electrode, and Ag wire as a reference in a drybox equipped with electrochemical outlets. CV's were recorded using a Bioanalytical Systems CV-27 voltammograph. All CV's were run at a scan rate of 100 mV/s with a sweep width of ±2 V. Solutions of the individual compounds were prepared by charging a via with 4 mg of compound and 0.400 g (1.03 mmol) of [*n*-Bu_4N][PF_6] and dissolving the solids in 10 mL of THF. This produced solutions of approximately 0.5 mM in compound and 0.1 M in electrolyte. After recording the baseline of a standard 0.1 M solution of electrolyte, CV's were collected for ferrocene and then for the compound. Oxidation potentials were then referenced to the formal potential of ferrocene.

Preparation of ^{iPr}APDI (4): A thick-walled glass vessel was charged with 0.910 g (5.58 mmol) of 2,6-diacetylpyridine, 25 mL of isopropylamine, and a stirbar. The vessel was sealed, submersed in liquid nitrogen, evacuated on a Schlenk line, placed in a 95 °C oil bath, and stirred for 48 hours. After this time, the contents of vessel were transferred into a 50 mL round bottom flask. Excess isopropylamine was removed in

vacuo yielding 0.600 g (44 %) of an orange oily solid identified by combined gas-chromatography and mass-spectroscopy and ^{1}H NMR spectrometry and as ^{iPr}APDI. GC/MS (m/z) calcd = 245, found 245. ^{1}H NMR (chloroform-*d*, 22 ˚C): δ 1.23 (d, 6.5 Hz, 12H, CH*Me*$_2$), 2.31 (s, 6H, backbone-Me's), 3.77 (sept, 6.5 Hz, 2H, C*H*Me$_2$), 7.25 (t, 7.5 Hz, 1H, p-Pyr), 8.35 (d, 7.5 Hz, 2H, m-Pyr). ^{13}C NMR (chloroform-*d*, 22 ˚C): δ 13.58 (backbone-Me's), 23.63 (CH*Me*$_2$), 51.74 (*C*HMe$_2$), 121.25 (m-Pyr), 136.75 (p-Pyr), 156.81 (o-Pyr), 164.05 (*C*=N).

Preparation of (^{iPr}APDI)FeBr$_2$ (4-Br$_2$): A 250 mL round bottom flask was charged with 0.500 g (2.04 mmol) of solid **4**, 0.439 g (2.04 mmol) of FeBr$_2$, and a stir bar. The flask was equipped with a needle valve and evacuated on a Schlenk line. Approximately 100 mL of anhydrous THF was added via vacuum transfer. The resulting yellow-green solution was stirred for 24 hours. Solvent from the now blue solution was removed in vacuo. The product was brought into the dry-box, suspended in a pentane solution, collected on a filter, washed with 3 x 20 mL of pentane, and dried in vacuo, yielding 0.891 g (94.9 %) of a blue solid identified as **4-Br$_2$**. Anal Calcd for $C_{15}H_{23}Br_2FeN_3$: C, 39.08; H, 5.03; N, 9.11. Found C, 38.18; H, 4.93; N, 7.84. Magnetic Susceptibility: μ_{eff} = 5.5 μB (solid state balance). ^{1}H NMR (dichloromethane-d_2, 22 ˚C): δ -11.49 (148, 6H, backbone-Me's), 0.40 (d, 840 Hz, 12H, CH*Me*$_2$), 32.46 (521, 1H, p-Pyr), 74.38 (194, 2H, m-Pyr), 176.04 (458, 2H, C*H*Me$_2$).

Preparation of (^{iPr}APDI)Fe(CO)$_2$ (4-(CO)$_2$): A thick walled glass vessel was charged with 9.924 g of mercury, ~30 mL of pentane, and a stir bar. A total of 0.050 g (2.17 mmol) of cut sodium metal was added to the vessel in ~20 mg pieces. The resulting slurry was stirred for 10 minutes to ensure complete dissolution of the metal. A

pentane slurry containing 0.200 g (0.43 mmol) of **4-Br$_2$** was added to the flask containing the amalgam. On the high-vacuum line, the vessel was evacuated and an atmosphere of carbon monoxide gas at liquid nitrogen temperature was added. The blue reaction mixture was stirred vigorously for 24 hours. Excess carbon monoxide was removed from the vessel on the high vacuum line. The green solution in the resulting mixture was decanted away from the amalgam. Pentane was used to extract the remaining product from the amalgam, and both portions were filtered through celite to remove NaCl. Solvent was removed in vacuo, yielding 0.024g (15%) of a green solid identified as **4-(CO)$_2$**. IR (pentane, 20 ˚C) ν_{CO}: 1852, 1956 cm^{-1}. ^{1}H NMR (benzene-d_6, 20 ˚C): δ 1.58 (d, 6.4 Hz, 6H, CHMe_2), 2.06 (s, 6H, backbone-Me's), 4.42 (q, 6 Hz, 2H, CHMe$_2$), 7.16 (t, 7.6 Hz, 1H, p-Pyr), 7.63 (d, 7.6 Hz, 2H, m-Pyr). ^{13}C NMR (benzene-d_6, 20 ˚C): δ 17.30, 19.20, 68.62, 116.81, 120.45, 129.23, 145.17, 146.70, 156.02.

Preparation of $^{(R)MePh}$APDI (5): A procedure for the synthesis of this compound has been reported.[20] However, a modification of the literature preparation was employed. A thick-walled glass vessel was charged with 1.505 g (11.47 mmol) of 2,6-diacetylpyridine, 6.98 g (57.35 mmol) of (R)-(+)-α-methyl-benzylamine, and a stirbar. The vessel was sealed, frozen over liquid nitrogen, evacuated on a Schlenk line, placed in a 95 °C oil bath, and permitted to stir for 96 hours. After this time, the contents of vessel were transferred into a 50 mL round bottom flask. Excess (R)-(+)-α-methyl-benzylamine was recycled for subsequent use. It was vacuum-distilled away from the product using a short-path distillation head. The remaining amine was removed in vacuo after addition of pentane to the residual oil. A total of 2.531 g (60 %) of an orange oil identified as $^{(R)MePh}$APDI was collected and used without further purification. ^{1}H NMR (chloroform-d, 22 ˚C): δ 1.58 (d, 6.5 Hz, 6H, CHPhCH_3), 2.48

(s, 6H, backbone-Me's), 4.95 (q, 2H, C*H*PhCH$_3$), 7.27 (t, 8 Hz, 2H, p-Ph), 7.37 (t, 8 Hz, 4H, m-Ph), 7.52 (d, 8 Hz, 4H, o-Ph), 7.77 (t, 8 Hz, 1H, p-Pyr), 8.28 (d, 8 Hz, 2H, m-Ar).

Preparation of ($^{(R)MePh}$APDI)FeBr$_2$ (5-Br$_2$): This compound was prepared using the method described for **4-Br$_2$** using 2.531 g (6.85 mmol) of an oil of **5** and 1.477 g (6.85 mmol) of $FeBr_2$, yielding 3.815 g (95.2 %) of a blue solid identified as **5-Br$_2$**. Anal Calcd for $C_{25}H_{27}Br_2FeN_3$: C, 51.31; H, 4.65; N, 7.18. Found C, 51.54; H, 4.80; N, 6.77.[31] Magnetic Susceptibility: μ_{eff} = 5.3 μB (solid state balance). ^{1}H NMR (chloroform-*d*, 22 °C): δ -16.28 (198, 6H, backbone-Me's), -0.46 (520, 8H, o/m-Ph), 1.96 (174, 8H, o/m-Ph), 5.87 (d, 197 Hz, 6H, CHPhC*H*$_3$), 9.10 (212, 2H, p-Ph), 38.20 (176, 1H, p-Pyr), 73.57 (172, 2H, m-Pyr), 153.03 (465, 2H, C*H*PhCH$_3$).

Preparation of ($^{(R)MePh}$APDI)Fe(CO)$_2$ (5-(CO)$_2$): This compound was prepared using the method described for **4-(CO)$_2$** using 9.772 g of mercury, ~30 mL of pentane, 0.049 g (2.13 mmol) of sodium metal, and 0.211 g (0.427 mmol) of **5-Br$_2$**, yielding 0.089g (43%) of a green solid identified as **5-(CO)$_2$**. IR (pentane, 20 °C) ν_{CO}: 1847, 1946 cm^{-1}. IR (KBr, 23 °C) ν_{CO}: 1874, 1945 cm^{-1}. ^{1}H NMR (benzene-d_6, 20 °C): δ 1.95 (d, 6.8 Hz, 6H, CHPh*Me*), 1.97 (s, 6H, backbone-Me's), 5.86 (q, 6.2 Hz, 2H, C*H*PhMe), 7.02 (t, 2.8 Hz, 2H, p-Ph), 7.06-7.14 (m, 9H, o/m-Ph & p-Pyr), 7.59 (d, 7.6 Hz, 2H, m-Pyr). ^{13}C NMR (benzene-d_6, 20 °C): δ 17.30, 19.20, 68.62, 116.81, 120.45, 129.23, 145.17, 146.70, 156.02.

Preparation of $^{(R)MeCy}$APDI (6): This compound was prepared in the same manner as **5**, using 0.930 g (7.09 mmol) of 2,6-diacetylpyridine and 4.51 g (35.40 mmol) of (R)-(-)-1-cyclohexyl-ethylamine, yielding 1.934 g (64 %) of an orange oil identified as

$^{(R)MeCy}$APDI. The compound was characterized by 1H NMR spectroscopy and high-resolution mass-spectroscopy. It was used without further purification. MS (m/z) calcd = 381.3144 found = 381.3136. ^{1}H NMR (chloroform-*d*, 22 ˚C): δ 0.89-1.07 (m, 4H, Cy), 1.15 (d, 6.5 Hz, 6H, CHCyC*H*$_3$), 1.19-1.39 (m, 6H, Cy), 1.46-1.59 (m, 2H, Cy), 1.69 (t, 13 Hz, 4H, Cy), 1.77 (d, 13 Hz, 4H, Cy), 1.86 (d, 13 Hz, 2H, Cy), 2.39 (s, 6H, backbone-Me's), 3.49 (p, 6.5 Hz, 2H, C*H*CyCH$_3$), 7.70 (t, 7 Hz, 1H, p-Pyr), 8.12 (d, 7 Hz, 2 H, m-Pyr). ^{13}C NMR (chloroform-*d*, 22 ˚C): δ 13.68 (backbone-Me's), 18.62 (CHCy*C*H$_3$), 26.57 (Cy), 26.66 (Cy), 26.91 (Cy), 30.00 (Cy), 30.14 (Cy), 44.74 (Cy), 61.46 (*C*HCyCH$_3$), 121.21 (m-Pyr), 136.63 (p-Pyr), 156.94 (o-Pyr), 163.95 (*C*=N).

Preparation of ($^{(R)MeCy}$APDI)FeBr$_2$ (6-Br$_2$): This compound was prepared using the method described for **4-Br$_2$** using 1.890 g (4.96 mmol) of an oil of **6** and 1.069 g (4.96 mmol) of FeBr$_2$, yielding 2.814 g (95.0 %) of a blue solid identified as **6-Br$_2$**. Magnetic Susceptibility: μ_{eff} = 4.9 μB (solid state balance). ^{1}H NMR (dichloromethane-d_2, 22 ˚C): δ -11.07 (703, 6H, backbone-Me's), -5.54 (275, 1H), -3.41 (240, 1H), -2.16 (577, 4H), -1.57 (83, 2H), -0.08 (49, 2H), 0.04 (49, 2H), 0.34 (47, 4H), 1.71 (d, 47 Hz, 6H, CHCyC*H*$_3$), 1.81 (m, 2H), 2.12 (40, 4H), 23.18 (35, 1H, p-Pyr), 77.21 (86, 2H, m-Pyr), 218.37 (415, 2H, C*H*CyCH$_3$).

Preparation of ($^{(R)MeCy}$APDI)Fe(CO)$_2$ (6-(CO)$_2$) This compound was prepared in the same manner as **4-(CO)$_2$** using 23.084 g of mercury, ~50 mL of pentane, 0.116 g (5.04 mmol) of sodium metal, and 0.600 g (0.1.01 mmol) of **5-Br$_2$**, yielding 0.217g (44%) of a green solid identified as **6-(CO)$_2$**. IR (pentane, 23 °C) ν_{CO}: 1889, 1953 cm^{-1}. ^{1}H NMR (benzene-d_6, 20 ˚C): δ 0.52 (39, 2H, Cy), 1.08 (51, 2H, Cy), 1.40 (47, 8H, Cy), 1.49 (211, 2H, Cy), 1.60 (88, 4H, Cy), 1.69 (m, 1.67, 6H, CHCyC*H*$_3$), 2.04 (47, 2H, Cy), 2.15 (23, 6H, backbone-Me's), 2.49 (37, 2H, Cy), 3.95 (31, 2H, C*H*CyCH$_3$), 7.16

(t, 7 Hz, 1H, p-Pyr), 7.62 (20, 2H, m-Pyr). ^{1}H NMR (benzene-d_6, 0 °C): δ 0.49 (q, 11 Hz, 2H, Cy), 0.79-0.90 (m, 2H, Cy), 0.95-1.10 (m, 4H, Cy), 1.10-1.20 (m, 2H, Cy), 1.29-1.46 (m, 4H, Cy), 1.46-1.56 (m, 2H, Cy), 1.57-1.65 (m, 2H, Cy), 1.70 (d, 6Hz, 6H, CHCyCH_3), 2.01-2.07 (m, 1H, Cy), 2.11 (s, 6H, backbone-Me's), 2.18-2.23 (m, 1H, Cy), 2.45-2.56 (m, 2H, Cy) 3.95 (p, 6.5 Hz, 2H, CHCyCH$_3$), 7.17 (t, 7.5 Hz, 1H, p-Pyr), 7.61 (d, 7.5 Hz, 2H, m-Pyr). ^{13}C NMR (benzene-d_6, 20 °C): δ 16.44, 18.15, 21.17, 23.07, 26.52, 27.23 (strong), 30.57, 31.57, 32.04, 45.42, 46.63, 67.47, 116.19, 116.77, 199.60, 121.32, 145.72, 155.40.

Preparation of (^{Et}PDI)Fe(η_2,η_2-CH$_2$CHCHCH$_2$) (3-Butadiene): A thick walled glass vessel was charged with 31.80 g of mercury, ~100 mL of pentane, and a stir bar. Sodium metal (160 mg, 6.95 mmol) was added to the vessel in ~20 mg portions. The resulting slurry was permitted to stir for 10 minutes to ensure complete dissolution of the metal. A pentane slurry containing 0.768 g of **3-Cl$_2$** (1.39 mmol) was added to the flask containing the amalgam. On the high-vacuum line, the vessel was evacuated and 27.81 mmol of butadiene was added via calibrated gas bulb. The reaction mixture was stirred vigorously for 24 hours. Unreacted butadiene was removed from the vessel on the high vacuum line. The orange solution in the resulting mixture was decanted away from the amalgam. Pentane was used to extract the remaining product from the amalgam, and both portions were filtered through celite to remove NaCl. Solvent was removed in vacuo, affording an orange solid. The solid was recrystallized overnight from a pentane solution at -35 °C yielding 0.193 mg (26%) of red crystals identified as **3-(Butadiene)**. Anal Calcd for $C_{33}H_{41}N_3Fe$: C, 74.01; H, 7.72; N, 7.85. Found C, 73.89; H, 7.37; N, 7.46. ^{1}H NMR (benzene-d_6, 20 °C): δ 0.86 (t, 6.8 Hz, 6H, CH$_2$*Me*), 0.93 (t, 6.8 Hz, 6H, CH$_2$*Me*), 1.47 (q, 7.4 Hz, 2H, CH_2Me), 1.66 (q, 8.0 Hz, 2H, CH_2Me), 1.76 (s, 6H, backbone-Me's), 1.85 (q, 8.0 Hz, 2H, CH_2Me), 2.03 (q, 7.4 Hz,

2H, C*H*$_2$Me), 2.77 (2H, 16 Hz, *cis*-butadiene), 3.39 (d, 12.0 Hz, 2H, *trans*-butadiene), 4.50 (2H, 25 Hz, butadiene-C*H*'s), 6.97 (d, 10.8 Hz, 4H, m-Ar), 7.04 (t, 7.6 Hz, 2H, p-Ar), 7.50 (t, 7.6 Hz, 1H, p-Pyr), 8.11 (d, 7.6 Hz, 2H, m-Pyr). ^{13}C NMR (benzene-d_6, 20 ˚C): δ 14.36 (CH$_2$*Me*'s), 17.92 (backbone-Me's), 23.70 (*C*H$_2$Me's), 24.52 (*C*H$_2$Me's), 63.56 (butadiene-*C*H$_2$'s), 104.58 (butadiene-*C*H's) 117.43 (p-Pyr), 117.67 (m-Pyr), 126.09 (p-Ar), 126.20 (m-Ar), 135.98 (o-Ar), 149.34 (N-Ar), 151.31 (o-Pyr), 153.11 (C=N).

2.6 References

[1] Bolm, C.; Legros, J.; Le Paih, J.; Zani, L. *Chem. Rev*. **2004**, *104*, 6217.

[2] Britovsek, G. J. P.; Vernon C. Gibson, V. C.; Kimberley, B. S.; Peter J. Maddox, P. J.; McTavish, S. J.; Solan, G. A.; White, A. J. P.; Williams, D. J.; *Chem. Commun*., **1998**, 849.

[3] Small, B. L.; Brookhart, M.; Bennett, A. M. A.; *J. Am. Chem. Soc.* **1998,** 120, 4049.

[4] Enright, D.; Gambarotta, S.; Yap, G. P. A.; Budzelaar, P. H. M. *Angew. Chem., Int. Ed*. **2002**, *41*, 3873.

[5] Ingleson, M. J.; Pink, M.; Caulton, K. G. *J. Am. Chem. Soc*. **2006**, *128*, 4248.

[6] Bouwkamp, M. W.; Lobkovsky, E.; Chirik, P. J. *Inorg. Chem*. **2006**, *45*, 2.

[7] Bart, S. C.; Chlopek, K.; Bill, E.; Bouwkamp, M. W.; Lobkovsky, E.; Neese, F.; Weighardt, K.; Chirik, P. J. *submitted*.

[8] Small, B. L.; Brookhart, M.; *J. Am. Chem. Soc*. **1998**, *120*, 7143.

[9] Britovsek, G. J. P.; Bruce, M.; Gibson, V. C.; Kimberley, B. S.; Maddox, P. J.; Mastroianni, S.; McTavish, S. J.; Redshaw, C.; Solan, G. A.; Strömberg, S.; White, A. J. P.; Williams, D. J. *J. Am. Chem. Soc*. **1999**, *121*, 8728.

[10] Bart, S. C.; Lobkovsky, E.; Chirik, P. *J. Am. Chem. Soc.* **2004**, *126*, 13794.

[11] Bouwkamp, M. W.; Lobkovsky, E.; Chirik, P. J. *J. Am. Chem. Soc*. **2005**, *127*, 9660.

[12] Britovsek, G. J. P.; Mastroianni, S.; Solan, G. A.; Baugh, S. P. D.; Redshaw, C.; Gibson, V. C.; Andrew, J. P.; Williams, D. J.; Elsegood, M. R. J. *Chem. Eur. J*. **2000**, *6*, 2221.

[13] Abu-Surrah, A. S.; Lappalainene, K.; Piironen, U.; Lehmus, P.; Repo, T.; Leskela, M. J. *Organomet. Chem*. **2002**, *648*, 55.

[14] Esteruelas, M. A.; López, A. M.; Méndez, L.; Oliván, M.; Oñate, E. *Organometallics* **2003**, *22*, 395.

[15] Chen, Y.; Qian, C.; Sun, J. *Organometallics* **2003**, *22*, 1231.

[16] Kleigrewe, N.; Steffen, W.; Blömker, T.; Kehr, G.; Fröhlich, R.; Wibbeling, B.; Erker, G.; Wasilke, J.-C.; Wu, G.; Bazan, G. *J. Am. Chem. Soc*. **2005**, *127*, 13955.

[17] Gibson, V. C.; Long, N. J.; Oxford, P. J.; White, A. J. P.; Williams, D. J. *Organometallics* **2006**, *25*, 1932.

[18] Bianchini, C.; Mantovani, G.; Meli, A.; Migliacci, F.; Zanobini, F.; Laschi, F.; Sommazzi, A. *Eur. J. Inorg. Chem*. **2003**, 1620.

[19] Cherian, A. E.; Domski, G. J.; Rose, J. M.; Lobkovsky, E.; Coates, G. W. *Org. Lett.* **2005**, *7*, 5135.

[20] Bianchini, C.; Lee, H. M. *Organometallics* **2000**, *19*, 1833.

[21] In collaboration with the Coates group

[22] Condensation of 2,6-diacetylpyridine with tertbutylamine was also attempted, but could not be effected, most likely due to unfavorable steric interactions between the tertbutyl group and the pyridine ring. Notably, the chemical literature contains no reports of condensation of tertbutylamine with benzylic ketones.

[23] Morassi, R.; Bertinin, I.; Sacconi, L. *Coord. Chem. Rev.* **1973**, *11*, 343.

[24] Hansch, C.; Leo, A.; Taft, R. W. *Chem. Rev.* **1991**, *91*, 165.

[25] Archer, A. M.; Bart, S. C.; Trovitch, R. J.; Cortez, M. P.; Chirik, P. J. *Unpublished Results.*

[26] Gibson, V. C.; Spitzmesser, S. K.; *Chem. Rev.* **2003**, *103*, 283.

[27] Ittel, S. D.; Johnson, L. K.; Brookhart, M. *Chem. Rev.* **2000**, *100*, 1169.

[28] General conditions employed sofar: treatment of pentane, toluene, or ether solutions of dihalides at ambient temperature with either (a) an excess of five equivalents of (0.5 % by mass) sodium amalgam for up to 48 hours or (b) two equivalents of sodium triethylborohydride for up to five hours.

[29] Marco Bouwkamp observed that treatment of (^{iPr}PDI)Fe(CH_2SiMe_3) with hydrogen gas prompted reductive elimination of tetramethylsilane and permitted isolation of (^{iPr}PDI)Fe(H_2), which cleanly converted to (^{iPr}PDI)Fe(N_2)$_2$ upon exposure to a nitrogen atmosphere. However, exposure of other bis(imino)pyridine iron monoalkyl compounds would not effect C-H bond coupling, rendering this route ineffectual.

[30] ^{Me}PDI = 2,6-(2,6-$Me_2C_6H_3N$=CMe)$_2C_5H_3N$ $^{2,5\text{-}tBu}$PDI = 2,6-(2,5-$^tBu_2C_6H_3N$=CMe)$_2C_5H_3N$, and PDI = 2,6-(C_6H_5N=CMe)$_2C_5H_3N$.

[31] Bart, S. C.; Chirik, P. J. *Unpublished Results.*

[32] Bart, S. C.; Lobkovsky, E.; Chirik, P. J. *Unpublished Results.*

[33] Bouwkamp, M. W.; Chirik, P. J. *Unpublished Results.*

[34] Bouwkamp, M. W.; Lobkovsky, E.; Chirik, P. J. *Unpublished Results.*

[35] Reihlen, H.; Gruhl, A.; von Hessling, G.; Pfrengle, O. *Justus Liebigs Ann. Chem.* **1930**, *482*, 161.

[36] Mills, O. S.; Robinson, G. *Acta Crystallogr.* **1963**, *16*, 758.

[37] Branchadell, V.; Deng, L.; Ziegler, T. *Organometallics*, **1994**, *13*, 3115.

[38] González-Blanco, Ó.; Branchadell, V. *Organometallics* **1997**, *16*, 475.

[39] Schroeder, M. A.; Wrighton, M. S. *J. Am. Chem. Soc*. **1976**, *98*, 551.

[40] Pangborn, A. B.; Giardello, M. A.; Grubbs, R. H.; Rosen, R. K.; Timmers, F. J. *Organometallics* **1996**, *15*, 1518.